Accepted Manuscript

2-(2-(2,4-dioxopentan-3-ylidene)hydrazineyl)benzonitrile as novel inhibitor of receptor tyrosine kinase and PI3K/AKT/mTOR signaling pathway in glioblastoma

Anisha Viswanathan, Dinesh Kute, Aliyu Musa, Saravanan Konda Mani, Vili Sipilä, Frank Emmert-Streib, Fedor I. Zubkov, Atash V. Gurbanov, Olli Yli-Harja, Meenakshisundaram Kandhavelu

PII: S0223-5234(19)30031-5

DOI: https://doi.org/10.1016/j.ejmech.2019.01.021

Reference: EJMECH 11028

To appear in: *European Journal of Medicinal Chemistry*

Received Date: 16 November 2018

Revised Date: 9 January 2019

Accepted Date: 9 January 2019

Please cite this article as: A. Viswanathan, D. Kute, A. Musa, S.K. Mani, V. Sipilä, F. Emmert-Streib, F.I. Zubkov, A.V. Gurbanov, O. Yli-Harja, M. Kandhavelu, 2-(2-(2,4-dioxopentan-3-ylidene)hydrazineyl)benzonitrile as novel inhibitor of receptor tyrosine kinase and PI3K/AKT/mTOR signaling pathway in glioblastoma, *European Journal of Medicinal Chemistry* (2019), doi: https://doi.org/10.1016/j.ejmech.2019.01.021.

RTK inhibitor

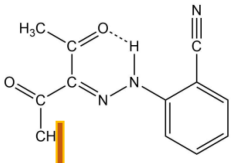

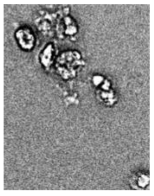

RTK Signaling Pathways genes affected by R234 in GBM

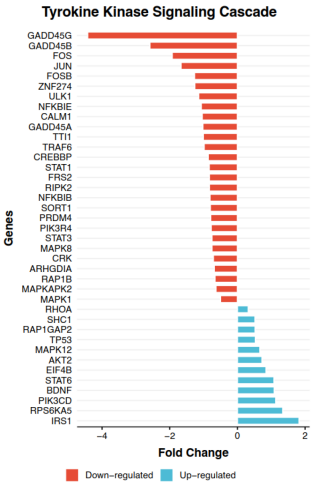

Apoptosis and Cell Cycle Arrest in GBM

2-(2-(2,4-dioxopentan-3-ylidene)hydrazineyl)benzonitrile as novel inhibitor of receptor tyrosine kinase and PI3K/AKT/mTOR signaling pathway in glioblastoma

Anisha Viswanathan[1], Dinesh Kute[1], Aliyu Musa[2], Saravanan Konda Mani[3], Vili Sipilä[1], Frank Emmert-Streib[2], Fedor I. Zubkov[4], Atash V. Gurbanov[5,6] , Olli Yli-Harja[7,8], and Meenakshisundaram Kandhavelu[1,*]

[1]*Molecular Signaling Lab, Faculty of Medicine and Health Technology, Tampere University and BioMediTech, P.O. Box 553, 33101 Tampere, Finland.*

[2]*Predictive Medicine and Data Analytics Lab, Faculty of Medicine and Health Technology, Tampere University and BioMediTech, P.O. Box 553, 33101 Tampere, Finland.*

[3]*Centre of Advanced Study in Crystallography & Biophysics, University of Madras, Chennai – 600 025*

[4] *Organic Chemistry Department, Faculty of Science, Peoples' Friendship University of Russia (RUDN University), 6 Miklukho-Maklaya St., Moscow, 117198, Russian Federation*

[5]*Centro de Química Estrutural, Instituto Superior Técnico, Universidade de Lisboa, Av. Rovisco Pais, 1049–001 Lisbon, Portugal*

[6]*Department of Chemistry, Baku State University, Z. Xalilov Str. 23, Az 1148 Baku, Azerbaijan*

[7]*Computaional Systems Biology Group, Faculty of Medicine and Health Technology, Tampere University and BioMediTech, P.O. Box 553, 33101 Tampere, Finland.*

[8]*Institute for Systems Biology, 1441N 34th Street, Seattle, WA 98103-8904, USA*

Abstract

Nerve growth factor receptor (NGFR), a member of kinase protein, is emerging as an important target for Glioblastoma (GBM) treatment. Overexpression of NGFR is observed in many metastatic cancers including GBM, promoting tumor migration and invasion. Hydrazones have been reported to effectively interact with receptor tyrosine kinases (RTKs). We report herein the synthesis of 23 arylhydrazones of active methylene compounds (AHAMCs) compounds and their anti-proliferative activity against GBM cell lines, LN229 and U87. Compound **R234**, 2-(2-(2,4-dioxopentan-3-ylidene)hydrazineyl)benzonitrile, was identified as the most active anti-neoplastic compound, with the IC_{50} value ranging 87 µM - 107µM. Molecular docking simulations of the synthesized compounds into the active site of tyrosine receptor kinase A (TrkA), demonstrated a strong binding affinity with **R234** and concurs well with the obtained biological results. **R234** was found to be a negative regulator of PI3K/Akt/mTOR pathway and an enhancer of p53 expression. In addition, **R234** treated GBM cells exhibited the downregulation of cyclins, cyclin-dependent kinases and other key molecules involved in cell cycle such as CCNE, E2F, CCND, CDK6, indicating that **R234** induces cell cycle arrest at G1/S. **R234** also exerted its apoptotic effects independent of caspase3/7 activity, in both cell lines. In U87 cells, **R234** induced oxidative effects whereas LN229 cells annulled oxidative stress. The study thus concludes that **R234**, being a negative modulator of RTKs and cell cycle inhibitor, may represent a novel class of anti-GBM drugs.

INTRODUCTION:

Glioblastoma Multiforme (GBM) is WHO grade IV astrocytoma, representing a highly heterogeneous group of neoplasms that are among the most aggressive and challenging cancers to treat. Though highly heterogeneous, GBM shares common essential characteristics with other

tumors, such as, uncontrolled proliferation, evading of apoptosis, invasiveness, avoidance of immune surveillance, resistance to chemotherapy and Reactive Oxygen Species (ROS) generation and angiogenesis [1].

Receptor tyrosine kinases (RTKs) are important regulators of intracellular signal-transduction pathways mediating cellular processes, including metabolism, cell-cycle control, survival, proliferation, motility and differentiation, and are often deregulated in cancer[2,3]. RTKs consist of families of growth factor receptors such as the platelet-derived growth factor receptor (PDGFR), fibroblast growth factor receptor (FGFR), vascular endothelial growth factor receptor (VEGFR), and epidermal growth factor receptor (EGFR), nerve growth factor receptor (NGFR) and 15 other subfamilies. Most of the members of RTK family are strongly associated with oncological diseases through gain-of-function mutations or through receptor/ligand overexpression [4]. GBM being high in intratumoral heterogeneity exhibits amplification of RTK expression on tumor cells [5], affecting the sensitivity to various chemo treatments [6]. The main signalling pathways activated by RTKs are PI3K/Akt, Ras/Raf/ERK1/2 and signal transduction and activator of transcription (STAT) pathways [7].

Among several RTKs linked with cancer, the NGFR is found to be positively correlated with astrocytic gliomas and several reports suggests the role of NGFs in GBM growth [8–10]. NGFRs includes two distinct family of receptor Trks and p75NTR and are found to be differentially expressed in glioblastoma and are identified as effective drugable targets for GBM [8,11–15]. NGFR is a transmembrane receptor for the neurotrophin family. Neurotrophins regulate the proliferation and differentiation of neurons in the central nervous system via NGFRs by activating specific tyrosine kinase receptors which include TrkA, TrkB, and TrkC [12]. Recent reports suggest that inhibition of NGFR could be a therapeutic target considering its role

in cell proliferation and survival [16], differentiation, cell cycle progression [17], apoptosis [11,18], neurite outgrowth and retraction [19] myelination [20] cell migration and invasion. The NGF-NGFR cascade is reported to activate nuclear factor-κB (NF-κB), leading to inhibition of apoptosis [21]. NGFR is also involved in feedback regulation of P53 and it has been reported that down regulation of NGFR, induced p53-dependent apoptosis and cell growth arrest, as well as suppressed tumor growth [22]. Neurotrophin binding to NGFR activates the c-Jun N-terminal kinase (JNK) signalling cascade, resulting in the activation of p53 and expression of pro-apoptotic genes such as Bcl-2 [23]. Alternatively, combined activation of NGFR and tumor necrosis factor receptor member TRAF6 has been shown to promote downstream activation of NF-κB signalling, which primarily promotes cell survival [24]. Blockade of NGF/Trk signalling via anti-NGF antibodies or Trk inhibitors reduced cell proliferation and tumorigenesis in a muscarinic acetylcholine receptor-3 dependent manner, suggesting NGF as an potential target in tumor treatment and prevention [25,26].

Currently the most targeted molecules in GBM pathway are Protein kinase inhibitors such as Lonarfanib [27], Sorafenib [28], Topoisomerase targeting Irinotecan [29], PKC inhibitors such as Enzastaurin [30] and Integrin inhibitors such as Cilengitide [31] and RTK inhibitors. The use of small-molecule inhibitors targeted against EGFR (Cetuximab and Panitututmab) is a common anti-tumor therapeutic strategy [32–35]. Anti- PDGFR agent Imatinib has been shown to inhibit GBM cell proliferation and induces cell cycle arrest in the G1 phase of the cell cycle [36]. Similarly, inhibitors of IGFR can modify sensitivity to several chemotherapeutic agents [37–40]. There is still considerable need of more effective chemotherapeutics targeting RTK signaling pathways in GBM disease.

Hydrazones are a potential class of compounds for new drug development, considering its established properties as anticonvulsant [41–43], anti-depressant [44,45], analgesic [46,47], anti-inflammatory [46,48,49], anti-microbial [45], anti-mycobacterial [50], anti-tumoral [51,52] activities. Among several potential arylhydrazones, Di- and tri-organotin(IV) complexes of arylhydrazones of methylene active compounds have shown better anti-proliferative effect against the growth of HCT116 and HEPG2 cancer cells[53]. In addition, hydrazone derivatives were also identified as potential anti-prostate cancer compounds [54]. These compounds induces the apoptosis by caspase 9 and 3 activation [55,56]. Lanthanide chelation with hydrazone derivatives have also expressed higher cytotoxic effect on colon cancer [57]. More recently, we also studied effect of the panel of many hydrazone derivatives on multiple human brain astrocytoma cells and the results showed a better anti-proliferation effect at micro molar level[58]. Considering the prior studies on hydrazone derivatives as a potential anticancer compound and tyrosine kinase inhibitors[59,60] the current study intend to correlate the pharmacodynamic behavior of the top hydrazone derivative under evaluation, with the genomic data, to identify the key pathways affected in the anti-neoplastic behavior, specifically via tyrosine kinase inhibition.

METHODOLOGY

2.1 . *Chemistry*

A series of new 3-(2-(1-(dimethylamino)-1,3-dioxobutan-2-ylidene)hydrazineyl)-2-hydroxy-5-nitrobenzenesulfonic acid (**3, R212**), N,N-dimethyl-2-(2-(4-nitrophenyl)hydrazineylidene)-3-oxobutanamide (**16, R221**), 4-(2-(2,4,6-trioxotetrahydropyrimidin-5(2H)-ylidene)hydrazineyl)benzoic acid (**19, R156**), sodium 2-(2-(1,3-dioxo-1,3-diphenylpropan-2-

ylidene)hydrazineyl)benzenesulfonate (**20, R246**), ethyl 2-(2-(4-chlorophenyl)hydrazineylidene)-3-oxobutanoate (**21, R40**), 4-(2-(1-cyano-2-methoxy-2-oxoethylidene) hydrazineyl)benzoic acid (**22, R313**), 5-(2-(2,4-dioxopentan-3-ylidene)hydrazineyl)isophthalic acid (**23, R283**) and known, 3-(2-(2,4-dioxopentan-3-ylidene)hydrazineyl)-2-hydroxy-5-nitrobenzenesulfonic acid (**1, R2**), triaqua[2-(hydroxy-κ*O*)-5-nitro-3-{2-[2-oxo-4-(oxo-κ*O*)pentan-3-ylidene]hydrazinyl-κN^1} benzenesulfonato(2-)]iron trihydrate (**2, FeR2**), (2-(2-(2,4-dioxopentan-3-ylidene)hydrazineyl) phenyl)arsonic acid (**4, R10**), 5-chloro-3-(2-(1-ethoxy-1,3-dioxobutan-2-ylidene)hydrazineyl)-2-hydroxybenzenesulfonic acid (**5, R31**), 2-hydroxy-5-nitro-3-(2-(2,4,6-trioxotetrahydropyrimidin-5(2H)-ylidene)hydrazineyl)benzenesulfonic acid (**6, R142**), 5-(2-(1,3-dioxo-1-phenylbutan-2-ylidene)hydrazineyl)-4-hydroxybenzene-1,3-disulfonic acid (**7, R46**), 2-(2-(2,4-dioxopentan-3-ylidene)hydrazineyl) benzenesulfonic acid (**8, R237**), 4-(2-(2,4-dioxopentan-3-ylidene)hydrazineyl)benzonitrile (**9, R241**), 2-(2-(2,4-dioxopentan-3-ylidene)hydrazineyl)benzonitrile (**10, R234**), 2-(2-(2,4-dioxopentan-3-ylidene)hydrazineyl) benzoic acid (**11, R236**), 3-(2-(2-nitrophenyl) hydrazineylidene)pentane-2,4-dione (**12, R235**), 3-(2-(4-chlorophenyl)hydrazineylidene)pentane-2,4-dione (**13, R8**), 3-(2-(4-bromophenyl)hydrazineylidene) pentane-2,4-dione (**14, R9**), ethyl 2-(2-(4-cyanophenyl) hydrazineylidene)-3-oxobutanoate (**15, R243**), 2-(2-(4,4-dimethyl-2,6-dioxocyclohexylidene) hydrazineyl)benzoic acid (**17, R244**), 2-(2-(2-hydroxy-4-nitrophenyl) hydrazineylidene)-1-phenylbutane-1,3-dione (**18, R48**) arylhydrazones of active methylene compounds (AHAMCs) have been prepared. Synthesis scheme of know compound is give in the supplemental file 1 while novel compounds synthesis scheme is given below.

2.2. Synthesis of novel arylhydrazone derivatives

The aryl hydrazones R212, R221, R156, R246, R40, R313 and R283 were synthesized via

Japp−Klingemann reaction[61–67][68–74] between the substituted aryldiazonium chloride and active methylene compounds in water solution containing sodium hydroxide (Table 1).

2.2.1. Diazotization

0.025 mol of substituted aniline was dissolved in 50 mL of water and then 0.025 mol of crystalline NaOH was added. The solution was cooled in an ice bath to 273 K and then 0.025 mol of $NaNO_2$ was added; after that 5.00 mL (33 %) HCl was added in portions for 1 h. The temperature of the mixture should not exceed 278 K. The resulting diazonium solution was used directly in the following coupling procedure.

2.2.2. Coupling

0.025 mol of NaOH was added to a mixture of 0.025 mol of active methylene compound with 50 mL of water. The solution was cooled in an ice bath to *ca*. 273 K, and a suspension of aryldiazonium chloride (see above) was added in three portions under vigorous stirring for 1 h

3, R212: yield, 77 % (based on N,N-dimethyl-3-oxobutanamide), yellow powder, soluble in water, methanol, ethanol, and insoluble in chloroform. Anal. Calcd for $C_{12}H_{14}N_4O_8S$ (M = 374.3): C, 38.50; H, 3.77; N, 14.97. Found: C, 38.42; H, 3.64; N, 14.84 %. IR, cm^{-1}: 3459 ν(OH), 2944 ν(NH), 1681 ν(C=O), 1628 ν(C=O···H), 1535 ν(C=N), 742 δ(C−H, Ar). ^{1}H NMR of a mixture of enol-azo and hydrazo tautomers, (300.13 MHz, D_2O). Enol-azo, δ: 2.55 CH_3, 2.97 and 3.08 $N(CH_3)_2$, 7.98−8.11 (2H, C_6H_2). Hydrazo, δ: 2.32 CH_3, 3.13 and 3.18 $N(CH_3)_2$, 7.98−8.11 (2H, C_6H_2). ^{1}H NMR of a mixture of enol-azo and hydrazo tautomers, (300.13 MHz, DMSO-d_6). Enol-azo, δ: 2.47 CH_3, 2.77 and 2.96 $N(CH_3)_2$, 7.98−8.18 (2H, C_6H_2), 9.94 (s, 1H, HO–Ar), 11.96 (s, 1H, HO-enol). Hydrazo, δ: 2.28 CH_3, 3.02 and 3.10 $N(CH_3)_2$, 7.98−8.18 (2H,

C_6H_2), 9.94 (s, 1H, HO–Ar), 13.60 (s, 1H, NH). $^{13}C\{^1H\}$ NMR (100.61 MHz, DMSO-d_6). Enol-azo, δ: 24.7, 34.0 and 34.8 (CH_3), 109.1 (Ar−N=N), 116.2 (C–N), 125.6 and 131.6 (2Ar−H), 136.4 (Ar−SO_3H), 139.7 (Ar−NO_2), 146.8 (Ar−OH), 162.0 (CH_3C−O), 194.5 ($N(CH_3)_2C$=O). Hydrazo, δ: 28.8, 37.3 and 38.1 (CH_3), 116.9 and 123.5 (2Ar−H), 123.5 (Ar−NH−N), 130.7 (Ar−SO_3H), 132.2 (C=N), 139.6 (Ar−NO_2), 145.4 (Ar−OH), 194.5 ($N(CH_3)_2C$=O), 196.0 (CH_3C=O). ^1H NMR of a mixture of enol-azo and hydrazo tautomers, (300.13 MHz, CD_3OD). Enol-azo, 2.54 CH_3, 2.92 $N(CH_3)_2$, δ: 8.23−8.36 (2H, C_6H_2). Hydrazo, δ: 2.34 CH_3, 3.18 and 3.18 $N(CH_3)_2$, 8.23−8.36 (2H, C_6H_2). $^{13}C\{^1H\}$ NMR (100.61 MHz, CD_3OD). Enol-azo, δ: 24.8, 29.8 and 34.7 (CH_3), 107.5 (Ar−N=N), 109.2 (C–N), 117.9 and 121.0 (2Ar−H), 133.4 (Ar−SO_3H), 140.5 (Ar−NO_2), 148.0 (Ar−OH), 164.5 (CH_3C−O), 196.7 ($N(CH_3)_2C$=O). Hydrazo, δ: 28.8, 38.2 and 38.8 (CH_3), 110.7 and 111.1 (2Ar−H), 112.3 (Ar−NH−N), 118.4 (Ar−SO_3H), 133.2 (C=N), 134.8 (Ar−NO_2), 141.8 (Ar−OH), 196.7 ($N(CH_3)_2C$=O), 200.4 (CH_3C=O).

16, R221: yield 72 % (based on N,N-dimethyl-3-oxobutanamide), orange powder soluble in DMSO, methanol, ethanol and acetone, and insoluble in water. Elemental analysis: $C_{12}H_{14}N_4O_4$ (M = 278.27); C 51.75 (calc. 51.80); H 5.02 (5.07); N 20.08 (20.13) %. IR (KBr): 2930 ν(NH), 1663 ν(C=O), 1634 ν(C=O···H), 1595 ν(C=N) cm^{-1}. ^1H-NMR in DMSO-d_6, δ (ppm): 2.42 (3H, CH_3), 2.78 (3H, CH_3), 2.99 (6H, CH_3), 7.38−7.49 (4H, Ar−H), 12.68 (1H, N−H). ^{13}C-$\{^1H\}$ NMR in DMSO-d_6, δ (ppm): 24.4 (CH_3), 33.7 (CH_3), 36.4 (CH_3), 116.1 (2Ar−H), 126.0 (2Ar−H), 129.1 (C=N), 138.4 (Ar−NO_2), 142.4 (Ar−NH−N), 163.3 and 194.3 (C=O).

19, R156: yield, 67 % (based on barbituric acid), yellow powder, soluble in water, methanol, ethanol, and insoluble in chloroform. Anal. Calcd for $C_{11}H_8N_4O_5$ (M = 276.20): C, 47.83; H, 2.92; N, 20.28. Found: C, 47.65; H, 2.90; N, 20.11 %. IR, cm^{-1}: 3365 ν(OH), 3214, 3019, 2855

ν(NH), 1715 ν(C=O), 1657 ν(C=O), 1592 ν(C=O···H), 1563 ν(C=N). ^{1}H NMR (300.13 MHz, DMSO-d_6) δ: 7.94−8.21 (4H, C_6H_4), 11.35 (s, 1H, NH), 11.54 (s, 1H, NH) and 14.31 (s, 1H, NH). ^{13}C{^{1}H} NMR (100.61 MHz, DMSO-d_6) δ: 111.3 and 117.9 (4Ar−H), 125.4 (Ar−COOH), 136.2 (C=N), 146.8 (Ar−NH−N=), 151.8, 157.6, 159.1 and 163.9 (C=O).

20, R246: yield 64 % (based on 1,3-diphenylpropane-1,3-dione), grey powder is soluble in DMSO, methanol, ethanol and acetone, and insoluble in hexane. Elemental analysis: $C_{21}H_{15}N_2NaO_5S$ (M = 43041; C 58.45 (calc. 58.60); H 3.43 (3.51); N 6.34 (6.51) %. IR (KBr): 3450 ν(OH), 3045 ν(NH), 1681 ν(C=O), 1607 ν(C=O···H), 1587 ν(C=N) cm^{-1}. ^{1}H-NMR in DMSO, internal TMS, δ (ppm): 7.12−7.98 (14H, Ar−H), 13.42 (s, 1H, N−H). ^{13}C-NMR in DMSO, internal TMS, δ (ppm): 125.42 (Ar−H), 127.13 (Ar−H), 128.25 (Ar−H), 128.36 (Ar−H), 128.43 (Ar−H), 128.56 (Ar−H), 128.90 (Ar−H), 129.49 (Ar−H), 130.38 (Ar−H), 132.43 (Ar−H), 132.85 (Ar−H), 133.08 (Ar−H), 133.729 (Ar−H), 134.05 (Ar−H), 134.67 (C=N), 138.19 (Ar−CO), 137.21 (Ar−CO), 138.16 (Ar−NH−N), 146.45 (Ar−SO_3Na), 191.44 (C=O), 192.52 (C=O).

21, R40: yield 96% (based on ethyl 3-oxobutanoate), yellow powder soluble in DMSO, methanol, ethanol, chloroform and acetone, and insoluble in water. Elemental analysis: $C_{12}H_{13}ClN_2O_3$ (M = 268.70); C 53.55 (calc. 53.64); H 4.74 (4.88); N 10.37 (10.43)%. IR (KBr): 3453 (NH), 1676 (C=O), 1643 (C=O···H), 1610 (C=N) cm^{-1}. ^{1}H NMR in DMSO-d_6, δ (ppm): 1.31 (s, 3H, CH_3), 2.40 (s, 3H, CH_3), 4.04 (2H, CH_2), 7.23–7.76 (4H, Ar–H), 13.23 (s, 1H, N–H). ^{13}C–{^{1}H} NMR in DMSO-d_6, d (ppm): 13.29 (CH_3), 32.33 (CH_3), 60.48 (CH_2), 116.48 (2Ar–H), 119.24 (Ar–Cl), 134.20 (2Ar–H), 135.44 (C=N), 144.28 (Ar–NH–N), 196.12 (C=O), 197.66 (C=O).

22, R313: yield 87% (based on methyl 2-cyanoacetate), yellow powder soluble in DMSO, methanol, ethanol, chloroform and acetone, and insoluble in water. Elemental analysis: $C_{11}H_9N_3O_4$ (M = 247.21); C 53.38 (calc. 53.44); H 3.54 (3.67); N 16.95 (17.00)%. IR (KBr): 3470 (OH), 3349 (NH), 1670 (C=O), 1646 (C=O···H), 1614 (C=N) cm^{-1}. ^1H NMR in DMSO-d_6, δ (ppm): 3.56 (s, 3H, OCH_3), 7.28–7.86 (4H, Ar–H), 11.70 (s, 1H, O–H). 13.08 (s, 1H, N–H). $^{13}C–\{^1H\}$ NMR in DMSO-d_6, d (ppm): 58.20 (OCH_3), 116.40 (2Ar–H), 124.58 (Ar–COOH), 133.72 (2Ar–H), 135.13 (C=N), 145.04 (Ar–NH–N), 162.06 (C=O), 196.29 (C=O), 197.80 (C=O).

23, R283: yield 94% (based on pentane-2,4-dione), yellow powder soluble in DMSO, methanol, ethanol, chloroform and acetone, and insoluble in water. Elemental analysis: $C_{13}H_{12}N_2O_6$ (M = 292.25); C 53.37 (calc. 53.43); H 4.08 (4.14); N 9.46 (9.59)%. IR (KBr): 3378 (OH), 3290 (NH), 1668 (C=O), 1626 (C=O···H), 1607 (C=N) cm^{-1}. ^1H NMR in DMSO-d_6, δ (ppm): 2.43 (s, 3H, CH_3), 2.46 (s, 3H, CH_3), 8.13–8.31 (3H, Ar–H), 13.99 (s, 1H, N–H). $^{13}C–\{^1H\}$ NMR in DMSO-d_6, δ (ppm): 26.27 (CH_3), 31.29 (CH_3), 119.34 (2Ar–H), 126.76 (Ar–H), 134.02 (Ar–COOH), 135.45 (Ar–COOH), 136.18 (C=N), 141.80 (Ar–NH–N), 167.71 (C=O), 167.94 (C=O), 196.32 (C=O), 197.01 (C=O).

2.3. Computational assessment of Ligand-Receptor interaction

The structures of 23 ligands were drawn in SDF format using the tool Marvin Sketch [Marvin Draw 5.1.5, 2008, Chemaxon Ltd., Budapest]. The ligands were prepared for docking simulations using the LigPrep module of the Schrödinger suite of tools. Most probable tautomers and all possible stereo isomers were generated to study the activity of individual stereotypes of each ligand. In the final stage of LigPrep, compounds were minimized with OPLS-2001 Force

field [75]. The Human nerve growth receptor structure with PDBID 1HE7 (Resolution- 2 Å) is downloaded from Protein Data Bank [76]. The protein structure was prepared using the 'Protein Preparation Wizard' of the Schrödinger suite (Schrödinger, LLC, New York, NY, 2009). The docking grid on the receptor has been generated based on the co-crystallized ligand. Docking was performed on prepared receptor and 23 ligands by using the Glide docking program [Glide, version 5.5, Schrödinger, LLC, New York, NY, 2009].

2.4.Cell Culture

Human GBM cell lines, U87 cells were grown in Minimum Essential Medium (MEM, Product# 51416C, Sigma-Aldrich, St. Louis, MO) with 10% FBS 2mM sodium pyruvate (Product# S8636, Sigma-Aldrich, St. Louis, MO), 1% Penicillin-Streptomycin and 0.025mg/ml Amphotericin B. LN229 cells were cultured in Dulbecco's Modified Eagle Medium - high glucose (DMEM, Catalog# L0102, Biowest) containing 5% FBS (Product # F1051, Sigma-Aldrich, St. Louis, MO), 1% Penicillin-Streptomycin (Product # P4333, Sigma-Aldrich, St. Louis, MO) and 0.025mg/ml Amphotericin B (Sigma-Aldrich, St. Louis, MO). Cells were maintained at 37°C in a humidified incubator supplemented with 5% CO_2. Biological and technical repeats were used for each condition.

2.5.In vitro cytotoxicity assay

Cytotoxicity assay was performed to determine the cell growth inhibitory effect of the compounds following treatment for 48hrs on the GBM cell lines, U87 and LN229. This assay was performed in two stages. First, a high concentration, 100µM, was used for all the compounds as well as for the positive control Cisplatin (Sigma-Aldrich, USA). Following which, in the second stage, the compounds, which exhibited better activity in the previous step, were

selected, and different concentrations (100µM, 75µM, 50µM, 25µM, and 10µM) were used to determine the IC_{50} of each compound. Treated cells were harvested by centrifugation at 1200 rpm for 10min. Cell viability was determined using trypan blue staining, using a Countess II Automated Cell Counter (Thermo Fisher Scientific) to count the number of live and dead cells. The inhibition percentage of each sample was determined using the following formula to determine the dose-response curve. From the dose-response curve, IC_{50} value of each compound was calculated.

Mortality % was calculated using the following formula:

$$\text{Mortality (\%)} = \frac{Mean\ No.of\ untreated\ cells\ (DMSO\ control) - Mean\ No.of\ treated\ cells\ \times 100}{Mean\ No.of\ untreated\ cells\ (DMSO\ control)}$$

Double staining assay

U87 and LN229 cell lines were grown as described previously, for 24hrs, followed by treatment with IC_{50} value of **R234** and incubated for 48hrs. Negative (untreated) and positive (Cisplatin) controls were maintained. Apoptosis/necrosis detection was carried out using Annexin V FITC and PI (Thermo Fisher Scientific). The apoptosis determination was performed following the standard protocol from the manufacture. Briefly, the cells were cultured in 6 well-plate with the initial cell density of 7×10^5 cells/well. The cells were incubated for 48hrs with **R234**, positive control and untreated cells conditions and then harvested and washed in cold PBS. The cell pellets were then resuspended in 1X Annexin-binding buffer provided in the kit. Consequently, 5µL of FITC conjugated Annexin V and 1µL of the 100µg/ml PI working

solutions were added to the 100µL of cell suspension. The cells were incubated in dark for 15 min, at room temperature, after which the stained cells were observed for fluorescence to distinguish apoptotic cells. The image acquisition was done by using EVOS imaging system (ThermoFisher Scientific) with 20X objective magnification. Approximately 300 cells were used for each analysis.

2.6.Caspase Activity assay

In vitro caspase-3 and caspase-7 activity leading to apoptosis was determined using Caspase-Glo® 3/7 Assay Systems (Promega Corporation). The reagent was prepared as mentioned by the manufacturer. The U87and LN229 cells were grown overnight in a 96-well-plate and were treated with IC_{50} of R234. Negative control, positive control and blank (medium+ DMSO+ dye) were maintained. Cells were incubated at 37°C in a humidified incubator supplemented with 5% CO_2 for 5hrs and then equilibrated at room temperature for 30 min. 100µL of Caspase-Glo 3/7 reagent was added to 100µL of cells/well and was incubated in a dark-chamber. The luminescence signal was quantified (Chameleon Multi-label Detection Platform) at one hour after treatment. Magnitude of fold change in luminescence between treated and untreated cells were determined using the following formula:

$$Fold\ increase = \frac{F_{test} - F_{blank}}{F_{control} - F_{blank}}$$

2.7.Intracellular Redox potential test

To evaluate the redox potential of **R234**, a comparative test, using H_2O_2 and standard drug against untreated cells, was performed using H2DCFDA (Catalog no.# D399 Life Technologies, USA). The U87 and LN229 cells were grown overnight in a 96-well-plate and

were treated with IC_{50} of **R234** for 5hrs at 37°C in a humidified incubator supplemented with 5% CO_2. Negative control, positive control and blank were maintained. Baseline effect due to solvent was determined as well. After 5hrs of treatment, cells were harvested by centrifugation at 3000 rpm for 10min and incubated with 200µL of 2µMH2DCFDA for 30min at 37ºC in the CO_2 incubator. Cells were then washed with pre-warmed PBS and resuspended in 200µL of pre-warmed medium.100µL of suspension was then transferred to each well, in a 96-well plate and incubated at room temperature for 20min. Finally, fluorescence signal was measured using Chameleon Multi-label Detection Platform (Excitation 485 nm, Emission 535 nm).

2.8. Cell Cycle intervention test

To elucidate the effect of the newly synthesized compound on the cell cycle progression, **R234** was examined against U87 and LN229 cells. A cell density of 1×10^6 cells were grown overnight at 37°C in a humidified incubator supplemented with 5% CO_2, cells were exposed to **R234** at its IC_{50} concentration for 48hrs. The cells then were collected by trypsinization, washed with cold phosphate buffered saline (PBS) and pellet was resuspended in 100µL of cold PBS. Subsequently, the cell suspension was added with 900 µL of 70% ethanol and stored at 4°C for 30min. Following that, the cells were harvested by centrifugation at 3000rpm, rinsed again by centrifugation with 1mL cold PBS. The cells were then stained with 20µL of DNA fluorochrome PI in a solution containing Triton X-100 and RNase and incubated at 37°C in a humidified incubator supplemented with 5% CO_2, for 15 min. Finally, the fluorescence was detected by imaging using an EVOS FL Cell Imaging System.

2.9.RNA Isolation and Gene Expression Evaluation

Cell were incubated with IC_{50} of test compound and standard drug Cisplatin for 48hrs at 37°C

in a humidified incubator supplemented with 5% CO_2. A negative control was maintained as well. All conditions were conducted in triplicated RNA from all samples in profiling was isolated using same protocol. Total RNA of >9.25ng/uL was isolated using GeneJET RNA purification kit (Catalog no.#K0731), according to the manufacturer's instructions. The yield was then measured spectrophotometrically using NanoDrop-1000 (Thermoscientific, USA). After quantification, the cells were considered for quality assessment by TapeStation and expression assay by Illumina Next Seq High Output profiling followed by analysis and validation studies.

2.10. Statistical Analysis

All experiments described in the present study were performed as with three biological and technical repeats. The data were presented as the mean ± standard error of mean. Statistical analyses between two groups were performed by Student's t-test. Differences among multiple groups were tested by one-way analysis of variance following by a Dunnett's multiple comparison test (GraphPad Prism 7.04). $P<0.05$ was considered to indicate a statistically significant difference.

3. **RESULTS**

AHAMCs interaction with receptor tyrosine kinase, TrkA

AHAMCs **1-23** were prepared according to Scheme 1 (Figure 1.a). Purity of all compounds (≥ 95%) was verified by melting point, NMR, elemental analysis and mass spectrometry measurements (see Supporting Information). Structures of these compounds are presented in Table 1. To obtain a deeper insight into the mode of action of all the novel derivatives (**1-23**) docking study was carried out against human NGFR protein, receptor tyrosine kinase, TrkA**.** The Glide docking results of the TrkA of interest with 23 ligands were presented in the Figure 1.b.

The ligand **R234** shows better binding with the receptor compared with other 22 ligands with a highest Glide score (-4.12). **R234** forms interactions with 11 amino acid residues, which is shown as two-dimensional interaction diagram (Figure 1.c). There are six hydrophobic amino acid residues, three polar residues and two charged amino acid residues form interaction with the receptor. The amino acid residues 313LEU and 314ARG form hydrogen-bonding interactions with the R234. The hydrogen bonding interaction between the TrkA and R234 is shown with arrow marks in the two-dimensional ligand interaction diagram.

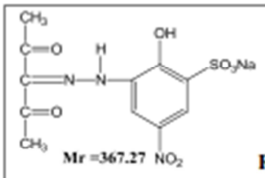 Mr =367.27 R_2 1	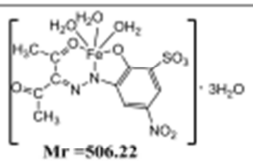 Mr =506.22 FeR2 2	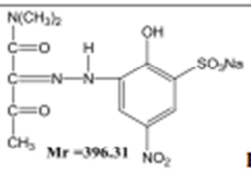 Mr =396.31 R_{212} 3
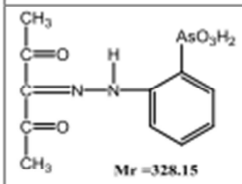 Mr =328.15 R_{10} 4	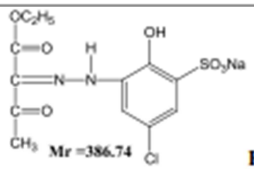 Mr =386.74 R_{31} 5	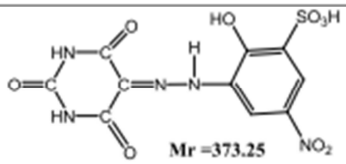 Mr =373.25 R_{142} 6
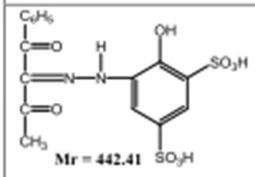 Mr = 442.41 R_{46} 7	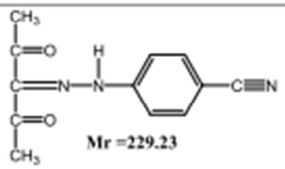 Mr =229.23 R_{241} 9	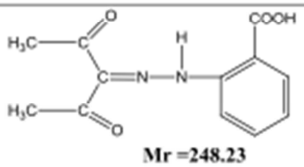 Mr =248.23 R_{236} 11
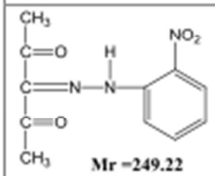 Mr =249.22 R_{235} 12	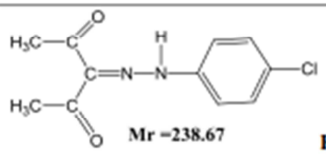 Mr =238.67 R_8 13	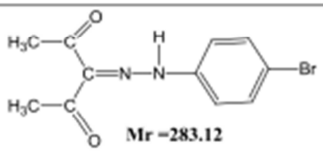 Mr =283.12 R_9 14
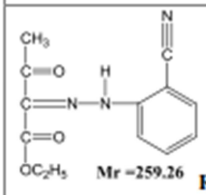 Mr =259.26 R_{243} 15	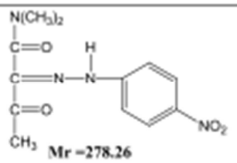 Mr =278.26 R_{221} 16	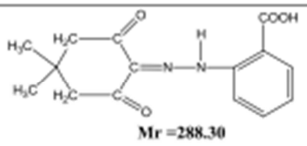 Mr =288.30 R_{244} 17
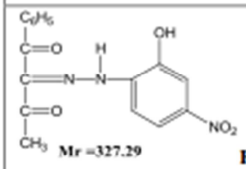 Mr =327.29 R_{48} 18	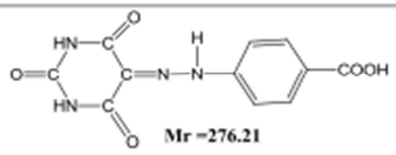 Mr =276.21 R_{156} 19	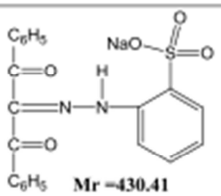 Mr =430.41 R_{246} 20
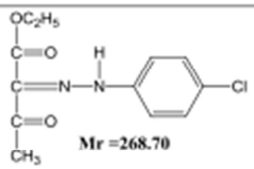 Mr =268.70 R_{40} 21	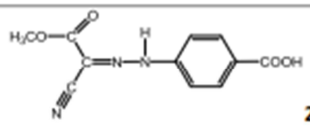 22 R313	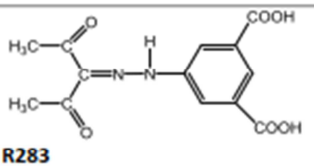 23 R283

Table 1. Arylhydrazones of active methylene compounds (AHAMCs).

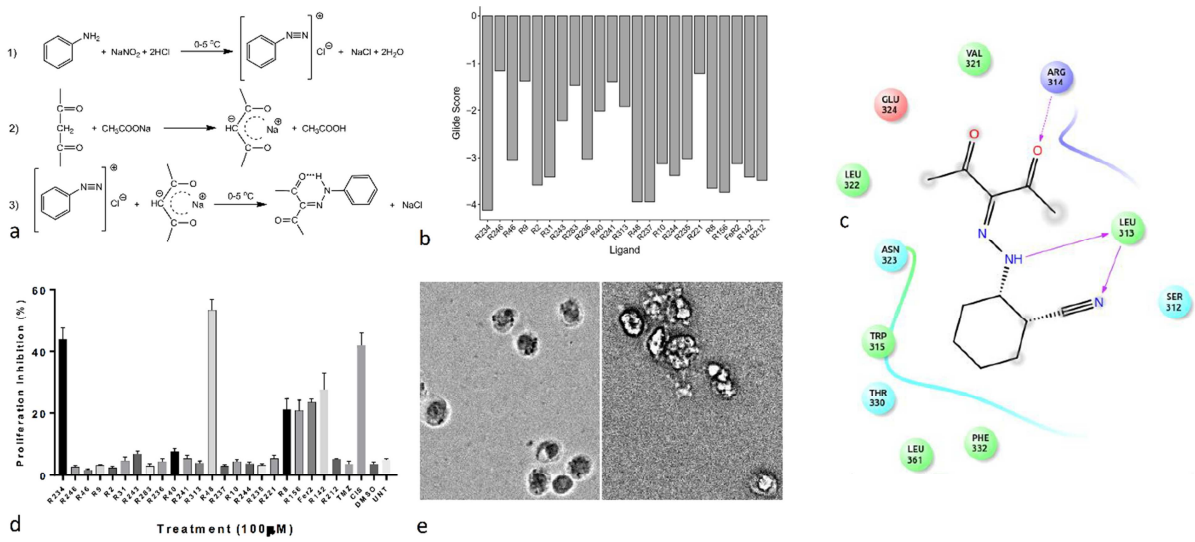

Figure 1: a. Scheme: Japp-Klingemann synthesis of hydrazones [61-74]. b. Docking scores of a panel of 23 novel aryl hydrazones of active methylene compounds (AHMACs) with tyrosine kinase TrkA. c. Structure activity relationship of R234 with TrkA receptor. d. Cytotoxicity assay of 23 AHAMCs in U87 cell line. e. Phase contrast image of U87 cells under apoptosis (non-apoptotic-left, apoptotic-right).

R234 Effectively reduces cell viability and Proliferation of GBM cells

To evaluate the efficiency of the AHMACs molecules as anti-GBM agents, effect on cell proliferation and viability was assessed for all synthesized compounds. Test compounds were initially screened against U87 cell line at 100uM concentration (Figure 1.d). Temolozamide and Cisplatin were used as positive control drugs and effects were evaluated against untreated cells. Baseline effect due to solvent was deducted. We have found the compound **R46** to have least cytotoxic activity. R234 and R48 induced higher anti-proliferative effect. However, docking of **R234** and R48 along with other compounds showed that **R234** has higher affinity than R48 with the TrkA receptor (Figure 1.b). Hence, the **R234** was further investigated to confirm the does- and time - dependent cytotoxic effect and found to be cytotoxic in GBM cell lines (Figure 1.e)

To generalize the potency of **R234** activity we used multiple GBM cell lines, LN229 and U87. The dose-response study was performed as described in the methods section and IC_{50} was determined for both cell lines. As expected, there was a gradient increase in mortality with increasing dosage in both cell lines, and IC_{50} value of **R234** was calculated as 107 µM in U87 and 87 µM in LN229, whereas IC_{50} value of Cisplatin was found to be 53 µM and 101 µM in U87 and LN229, respectively (Figure 2.a and b). Surprisingly, there was steady increase in cytotoxicity over first 48hrs whereas a loss in cytotoxic activity was observed after 48 hrs, in both U87 and LN229 cell lines) (Figure 2. c and d). In addition, R234 was also tested against the growth of normal brain cells (Mouse Embryonic Fibroblasts, MEF). At 100 µM treatment the cells expressed less than 20% death suggesting that R234 cytotoxic effect is specific to GBM cells (data not show).

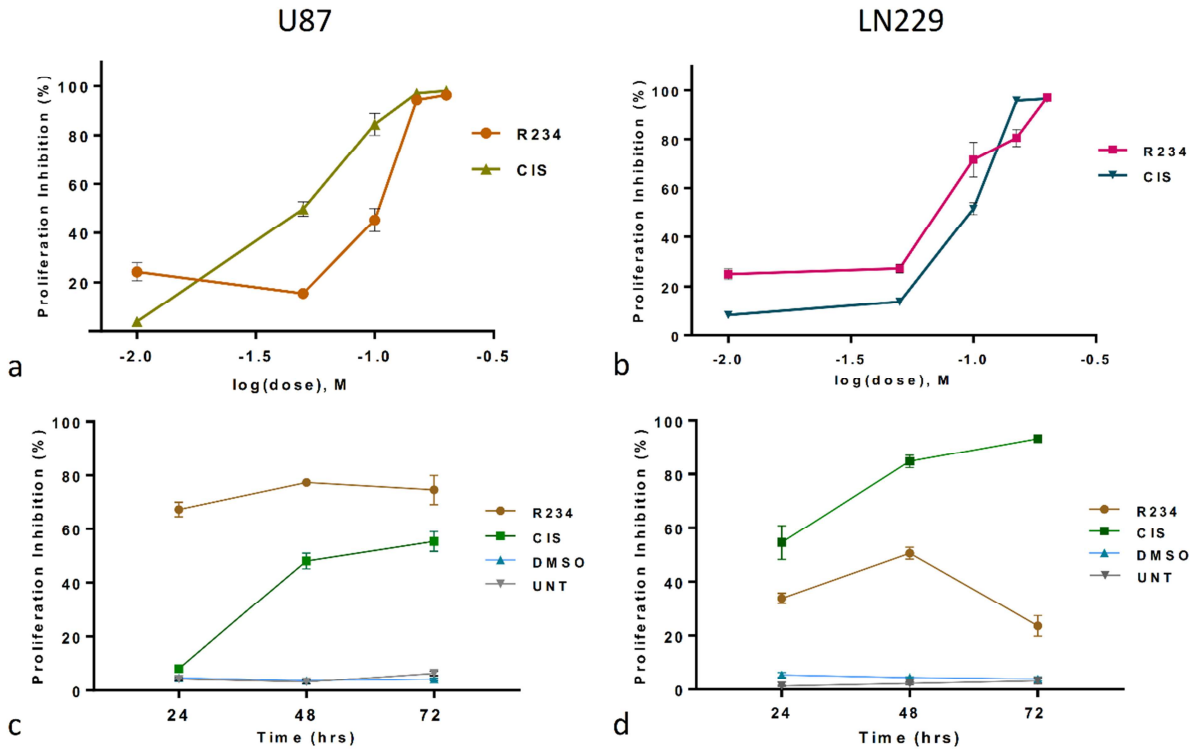

Figure 2: R234 inhibits GBM cell proliferation in a time and dose dependent manner. a. U87 cells were treated for 5hrs with 0-200 µM quantity of R234, after 24hrs of cell growth. Cellular viability was measured by the Trypan Blue exclusion method. Datapoints and error bars represent mean ± S.E.M (n = 4 per group). * $P < 0.05$ per one-way ANOVA. b. U87 cells were treated for 5hrs, with 0-200 µM quantity of R234, after 24 hrs of cell growth. Datapoints and error bars represent mean ± S.E.M (n = 4 per group). * $P < 0.05$ per one-way ANOVA. c. U87 cells were harvested after 24 hrs of cell growth and subsequently treated with IC_{50} value of R234 upto 72hrs. Proliferation Inhibition was monitored every 24hrs. Data points and error bars represent mean ± S.E.M (n = 4 per group). * $P < 0.05$ per one-way ANOVA. d. LN229 cells were harvested after 24hrs of cell growth and subsequently treated with IC_{50} value of R234 upto 72hrs. Proliferation Inhibition was monitored every 24hrs. Datapoints and error bars represent mean ± S.E.M (n = 4 per group). * $P < 0.05$ per one-way ANOVA

R234 Interrupts of Cell Cycle by inducing G1/S arrest

In order to investigate whether **R234** induces cell cycle disturbances in GBM cells, cell cycle analysis was performed using Propidium iodide staining method as described in method section, following **R234** treatment at IC_{50} for 24 h. Cells exhibit fluorescence bright red, proportionate to their DNA content in each cell phase (Figure 3.a and b). Significant G1/S transition arrest was observed in U87 cells treated with R234, with a concomitant reduction in the fraction of cells in S phase. Fraction of cells in G1 phase was 47.7% in **R234** treatment, 44.0% in positive control Cisplatin and 39.7% in untreated cells. In S phase, the percentage of the population was 2.8% in **R234** treatment, 5.6% in positive control and 19.2% in untreated cells (Figure 3.c). Baseline effect due to DMSO was negligible. However, in LN229, a similar trend of minimal cell fraction in S phase cells were observed, in treated condition in comparison to untreated condition. Particularly, higher fraction of cells at G1 phase in was observed in **R234** treatment. Low fraction of cells in G2/M in **R234** treated cells clearly indicates that the drug induces cell cycle arrest at G1/S (Figure 3.d).

Cell cycle gene expression analysis of U87 cell line revealed differential expression of 77 genes associated with G1-S phase, 82 in S phase and 74 in G2/M phase. Down regulation of ORCs (ORC1, ORC6) and MCMs (MCM3-7) were observed clearly indicating the blocking of

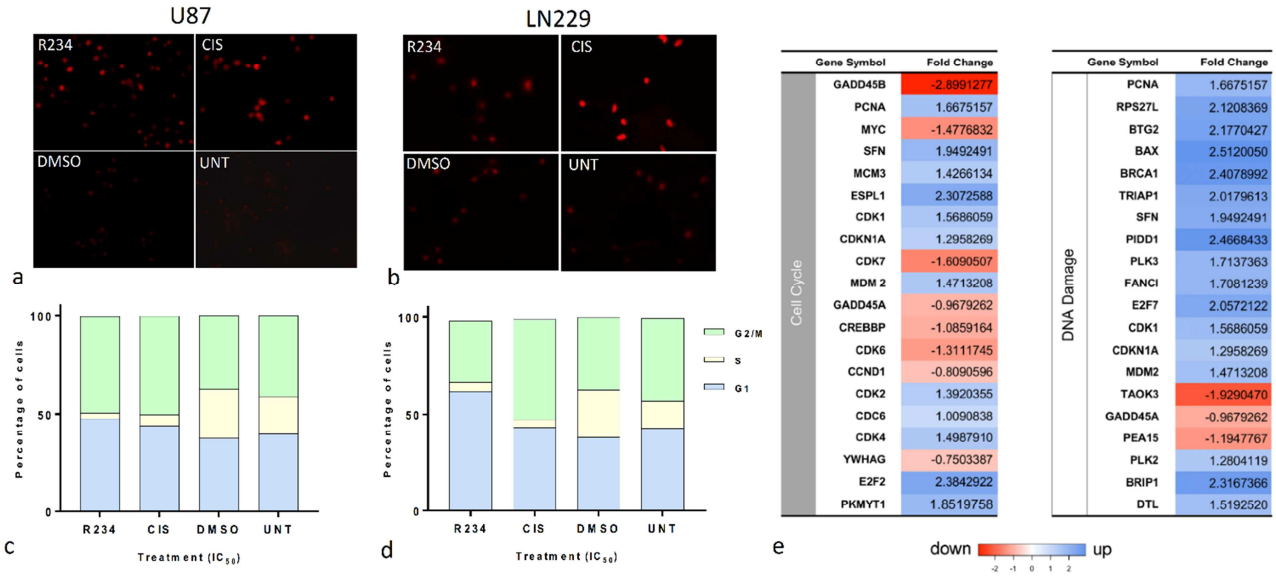

Cell Cycle	Gene Symbol	Fold Change
	GADD45B	-2.8991277
	PCNA	1.6675157
	MYC	-1.4776832
	SFN	1.9492491
	MCM3	1.4266134
	ESPL1	2.3072588
	CDK1	1.5686059
	CDKN1A	1.2958269
	CDK7	-1.6090507
	MDM 2	1.4713208
	GADD45A	-0.9679262
	CREBBP	-1.0859164
	CDK6	-1.3111745
	CCND1	-0.8090596
	CDK2	1.3920355
	CDC6	1.0090838
	CDK4	1.4987910
	YWHAG	-0.7503387
	E2F2	2.3842922
	PKMYT1	1.8519758

DNA Damage	Gene Symbol	Fold Change
	PCNA	1.6675157
	RPS27L	2.1208369
	BTG2	2.1770427
	BAX	2.5120050
	BRCA1	2.4078992
	TRIAP1	2.0179613
	SFN	1.9492491
	PIDD1	2.4668433
	PLK3	1.7137363
	FANCI	1.7081239
	E2F7	2.0572122
	CDK1	1.5686059
	CDKN1A	1.2958269
	MDM2	1.4713208
	TAOK3	-1.9290470
	GADD45A	-0.9679262
	PEA15	-1.1947767
	PLK2	1.2804119
	BRIP1	2.3167366
	DTL	1.5192520

DNA elongation. Gene expression analysis highlighted the P53 activation and subsequent downregulation of cyclins, cyclin-dependent kinases and other key molecules involved in cell cycle such as CCNE, E2F, CCND, CDK6 etc. (Figure 3.e). The high fraction of cell population in G1 phase in **R234** treated cells could be explained by the Rb mediated downregulation of Cyclin E (CCNE), which is required for the transition from G1 to S phase of the cell cycle.

Figure 3: R234 induces cell cycle arrest in GBM cells. Cells were treated with DMSO (negative control), Cisplastin (positive control) and R234 for 48hrs. Microscopic image analysis was performed for cell-cycle distribution. The DNA content was evaluated with Propidium iodide (PI) staining and fluorescence measured and analysed. **a.** Representative fluorescence microscopy images for each treated or untreated groups in U87, in S phase. **b.** Representative fluorescence microscopy images for each treated or untreated groups in LN229 cells. c**.** Percentage of U87 cells in various phases is fraction of whole population. d**.** Percentage of LN229 cells in various phases is fraction of whole population. Data represented as mean ± S.E.M of triplicates, *$p<0.05$ as compared with the control group. **e.** Fold change for the list of representative genes in the cell cycle and DNA damage pathways. The blue and red colors represent those genes that were upregulated and downregulated, respectively.

R234 induces apoptosis by negatively regulating stress protective mechanisms and DNA Damage Repair

Apoptosis assay was performed using Annexin V/PI test to determine the fraction of apoptotic cells. Apoptotic cells appeared bright red, necrotic cells as bright green and apo-nectrotic cells as bright orange (Figure 4.a). In U87 cell line, 68.7% of population under R234 treatment were found to be apoptotic, followed by 41.0% in Cisplatin treatment, and 22.4% in untreated cells (Figure 4.b). In LN229 cell line, this was 57.3% of the population under R234

treatment, followed by 32.6% in Cisplatin treatment, and 29.3% in untreated cells (Figure 4.c). Relevantly, the key differentially expressed genes involved in apoptotic process were identified

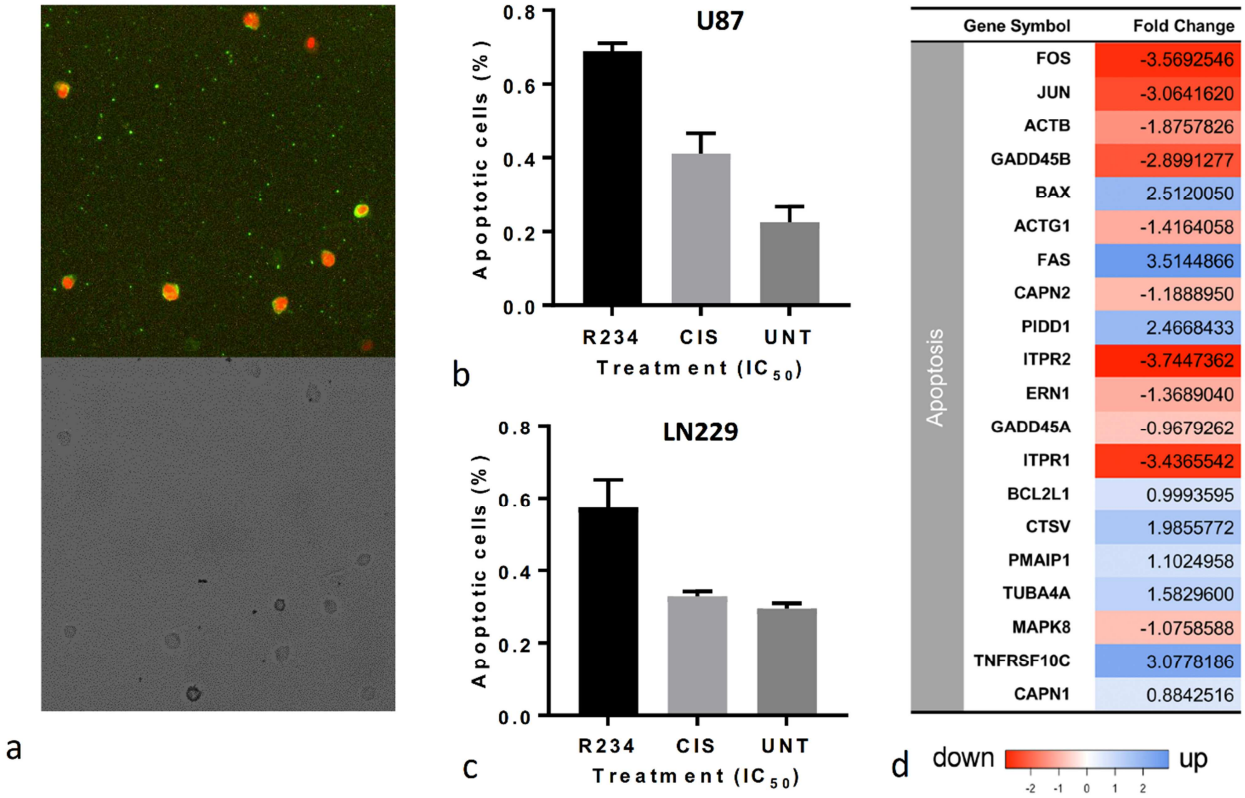

as FOS, JUN, ITPR, ACTB and ACTG1(Figure 4.d) Transcriptome analysis identified upregulation of pro-apoptotic genes such as NOXA, PUMA, BIM, and downregulation of IAPs, HSPs, (Supplementary file 2) that favours cell survival, suggesting the positive role **R234** in cancer cell apoptosis and chemosensitizing. Also, DNA repair genes such as GADD45s and SESNs were found to be notably downregulated. Genes such as TUBB3, ACTB, TESK1, PARVA, and ACTN1 were also found to be downregulated suggesting negatively affecting cellular integrity and survival. Stress response genes such as NQO1, GSTs and TrxR1 were also downregulated, which is sensitizes the cell to chemotherapy.

Figure 4: Annexin V/PI double-staining assay of GBM cells treated with R234 for 48h indicates that the drug effectively induced apoptosis as compared to control cells. **a**. Fluorocytogram of U87 cells exhibited upon Annexin V/PI double-staining (top). Phase contrast image of the treated cells(bottom). **b.** The histogram represents the percentage of PI_positive cells, in the U87 population. **c.** The percentage of PI positive cells, in the U87 population. **d.** Key genes involved in Apoptotic process and their Log2(Fold Change), that are differentially expressed upon R234 treatment, compared to untreated. *$p<0.05$ as produced by ANOVA test.

Reactive oxygen species (ROS) mediated caspase activation and subsequent cell death has been repeatedly reported by various studies [77–79]. Both intracellular ROS and caspase in U87 cells were quantified to assess redox flux as subsequent caspase activation due to the treatment with candidate molecule. The oxidative potential of **R234** was determined by ROS assay using H2DCFDA indicator as described in methods section. The results shows that oxidative stress increase of 9.5 % in the **R234** treated U87 cells when compared to untreated cells, whereas the standard drug cisplatin and positive control H_2O_2 marked 3.7% and 1.6 % respectively. However, in LN229 cell line there was no statistically significant difference found between treated and untreated cell (Figure 5.a). These results suggest that ROS may not played a major role in R234 induced GBM cell death.

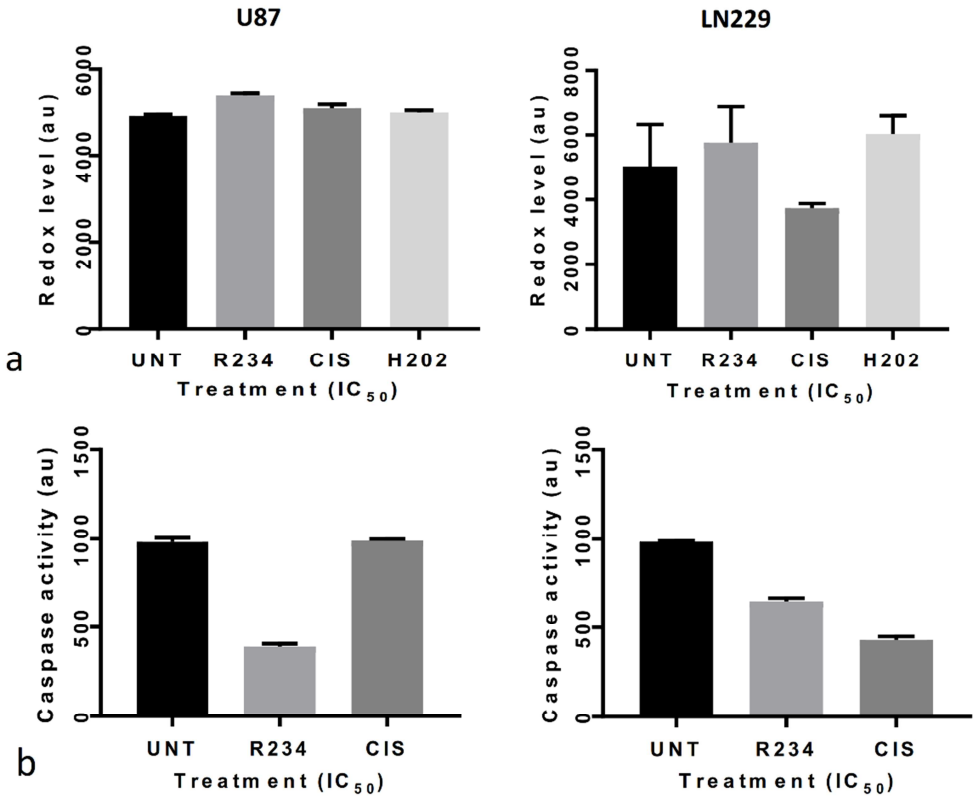

Figure 5: a. Effect of R234 on intracellular ROS production by GBM cells(U87 cells-left, LN229 cells-right). R234 treatment marginally increased cellular oxidation in both cell lines. **b**. Caspase activity displayed by GBM cells analyzed using caspase3/7 luminescence assay kit. Decrease in caspase activity of cells was observed after treatment with IC_{50} of R234 for 5hrs compared to control. The values are expressed as means ± SEM of triplicate measurements of at least two independent experiments. Significant differences compared between control and treated cells (*$p<0.05$).

Considering the role of ROS in caspase-mediated apoptosis, we determined the caspase activity of both cell lines using caspase 3/7 assay after a treatment period of 5hrs with IC_{50} of **R234**. Interestingly, U87 cells treated with **R234** displayed a reduction of caspase 3/7, displaying a decrease of 60.2% in comparison to untreated cancer cells, whereas positive control displayed

1.03% increase in caspase activity. In LN229, both candidate drug as well as positive control exhibited a reduction in caspase activity with 36.1% and 56.4% respectively (Figure 5.b). The difference between **R234** treated and untreated conditions, was confirmed to be statistically significant, per ANOVA test (P-value < 0.05). Over all, these observations suggest that ROS-independent and caspase-depended apoptosis is induced by R234.

Differentially expressed genes between GBM cells treated with R234 and control samples

In the DEGs analysis, 22,260 genes were mapped by at least one read in each sample profile. In total, 5,619 DEGs with a q-value < 0.05 and fold change > 1.5 were detected over the 2 comparisons of R234 with Untreated and R234 with Cisplatin in DESeq2 (Supplementary file 2). The numbers of differentially expressed genes with more than 2-fold change were higher in negative control. Therefore, there were higher number of differentially expressed genes in R234 cell line when analyzed with untreated cell line. We applied the MA plot function in DESeq2 to visualize the top genes with the smallest q-values (Figure 6.a). We investigated the similarity in differential gene expression profiles regulated untreated samples and Cisplatin treated samples. The fold-changes in overlapped genes filtered by the q-value < 0.05 were plotted for U87 cell line. Venn diagrams indicated overlap in genes whose expression was regulated in the same direction (Figure 6.b). The total number and up- or down-regulated number of DEGs (>=2-fold change, p-value 0.05) for untreated, Cisplatin and Both (Figure 6.c). We identified 3256 DEGs between R234 and Untreated (negative control) samples (q-value < 0.05). We also compared the R234 and Cisplatin samples as a positive control group, both individually and combined as a single “affected” group. In these comparisons, 2,442 number of DEGs were identified, with the largest number of DEGs identified in comparison with the untreated samples, and 1,321 out of 5,619 DEGs are common in both comparison (Supplementary file 2 and Figure 6.b). The

complete lists of DEGs from the cell line analysis and all pairs of comparisons are presented in Supplementary file 2.

R234 disrupt the functions and pathways of GBM

Pathway effects were elucidated by Gene Ontology analysis to analyze up and down regulated genes concerning DNA damage, cell cycle and apoptosis for R234 and untreated

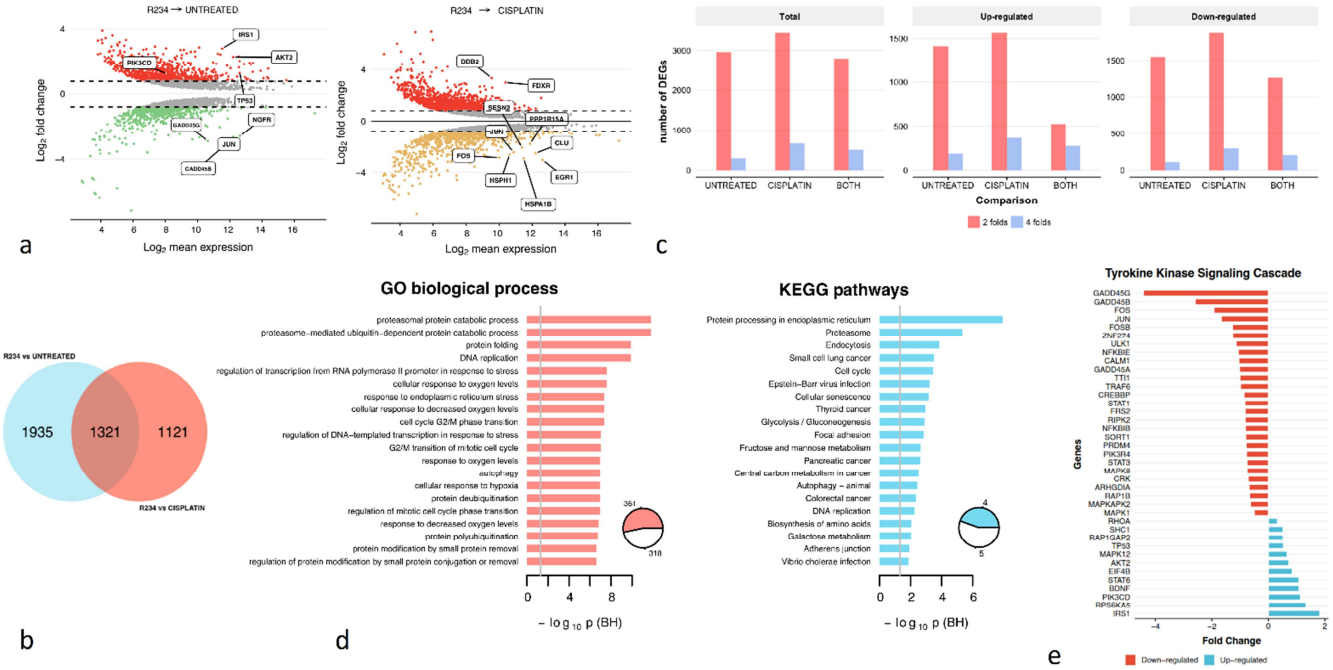

sample comparison. GO analysis identified the list of genes that were enriched in DNA replication, protein folding and regulation of transcription in response to stress. These biological processes are involved in the DNA replication pathway for Cisplatin (Figure 6.d left). Enrichment analysis for GO molecular function and pathways clearly demonstrated related phenotypes associated with GBM (Figure. 6.d right). GO terms cadherin binding, damaged DNA binding for molecular function appeared to be significantly overrepresented, and none significantly underrepresented. Cadherin binding, a type I membrane protein involved in cell adhesion and damaged DNA binding, interacting selectively and non-covalently with damaged DNA have coordinated effect on regulation and function in DNA damage (will discuss the list of pathways to add).

Figure 6: **a.** The MA-plot from means and log fold changes. It shows differential gene expression from the two inter-group comparisons (R224 vs. Untreated; R224 vs. Cisplatin). **b.** Overlapping DEGs in Untreated vs R234 and Cisplatin vs R234 compared. For the comparison, only genes with a q-value < 0.05 were considered as DEGs. The number of DEGs found at each comparison are indicated. **c.** The total number and up- or down-regulated number of DEGs (>= twofold change, p-value 0.05) for Untreated, Cisplatin and Both. **d.** Biological processes represented by the DEGs (<= twofold cutoff, p-value < 0.05) for R224 in comparison with untreated samples, using GO enrichment analysis. The percentage showed that the number of DEGs hit against total number of genes belonging to each GO terms in the categories(left). KEGG enrichment analysis identifying the most affected signaling pathways (>= twofold cutoff, p-value < 0.05) (right). **e.** RNA-Seq analysis of the expression representative of 40 genes by comparing the R224 and Untreated samples from the gene expression in U87 cell line. It shows the up- and down-regulated genes associated with Tyrokine Kinase Signaling cascade, and the log fold changes.

There were 3256 DEGs, including 1595 upregulated and 1661 downregulated DEGs, between **R234**-treated and untreated expression profiles. Interestingly, 1866 DEGs were found to have overrepresented in both in Cisplatin as well as **R234** treatment. Genes downregulated due to **R234** were enriched in KEGG pathways including Endocytosis, Cell cycle, Focal adhesion, p53 signaling pathway, Neurotrophin signaling pathway and cell cycle, whereas upregulated genes were associated with the pathways of Apoptosis, MAPK signaling pathway, Lysosome, Spingolipid signaling pathway and Proteoglycans in cancer(Supplementary file 2). Top20 overrepresented genes associated with significant processes such as cell cycle, DNA Damage and Apoptosis are given in Figure 5.c. It is interesting to note that following **R234** treatment, a

significant reduction in HSPs, IAPs, Proto-oncogenes, pro-survival genes as well as increase in pro-apoptotic genes were observed, suggesting increased chemo-sensitivity and low survival[80]. Also many of the genes providing cell stability was found to be downregulated such as TUBB3, ACTB, MCL1, PARP, SPTAN1, MITF etc (Supplementary file 2).

R234 exerts antiproliferation effects on GBM cells via RTK pathways

The molecular mechanisms of **R234**-mediated growth inhibition of GBM cells further investigated by gene expression analysis as described in method section. The effects of R234 on oncogenic RTK signaling were investigated using RNA seq analysis. R234 decreased the activation of significant genes in RTK pathway such as JUN, FOS, MAPK8 etc (Figure 6.e). Additionally many other significant genes involved in the pathway was found to be suppressed by R234, such as, mTOR, HIF1A, EIF4E, NRF2, MAP3K, GRB2, MAPK1, FOS and GSK3, while increasing TP53, RBL2, Bim, Noxa, Puma, HDAC etc. (Supplementary file 2). The major implication of RTK mediated anti-GBM effects are through AKT signaling, affecting mTOR cascade, P53 pathways, JNK pathway, FOXOs, IAPs and other significant molecules affecting cell cycle, growth, proliferation, cell survival and cellular metabolism (Supplementary file 2). One interesting observation was the downregulation of NGFR downstream signaling pathway genes such as PI3K, JNK, NF-kβ pathways demonstrating the potential of R234 to act as an antagonist of RTK pathways.

In detail, the gene expression analysis also revealed that **R234** significantly downregulates NGFR mediated signaling indicated by downregulation of MAP3K, GRB2, MKK3, and JNK1 (Supplementary file 2). This subsequently affects key genes such as mTOR and P53 via Akt signaling leading to cell cycle arrest, proliferation inhibition, anti-angiogenesis and chemo-sensitization, via multiple pathways. The PI3K/Akt/mTOR signaling pathway

promotes cellular growth, migration, protein synthesis, survival and metabolism in tumor cells [81–83]. The expression of PI3K/Akt/mTOR pathway was significantly reduced in **R234** treated cells, compared to control as evident from the gene expression profile.

DISCUSSION

Despite huge efforts being taken to develop potent drugs to fight glioblastoma, only a minority of patients benefit with currently approved chemotherapies. In the present study, we have demonstrated that a novel hydrazone derivative **R234** exerts cytotoxic, antiangiogenic and pro-apoptotic activity via RTK signaling pathways. **R234** demonstrated the effective anti-proliferative activity in a dose- and time-dependent manner. This observation is supported by earlier studies published on hydrazone derivatives as potent anti-tumor [84–88] agents.

Interestingly, **R234** exposure at an IC_{50} concentration for 24h caused cell cycle arrest at the G1/S phase and subsequent apoptosis, which may be a therapeutic aspect for its use in cancer chemotherapy. **R234** effectively reduces CCNE, CDK6 and E2Fs whereas upregulates RBL1 (RB family protein), which may explain the G1/S transition arrest. Cells advancement from G1 to S-phase irreversibly relies on cyclin E/cdk2 phosphorylation of pRB to release activator E2Fs that transcribe cyclin E [89]. Down regulation of CCNE thus negatively regulates G1 to S phase transition. The downregulation of MCMs and ORCs gene expression affecting the pre-replicative (pre-RC) complex demarks the origin to be licensed, to be triggered and initiate DNA synthesis. Also it has been shown that, pRB can physically localize to replication origins in S-phase to arrest DNA synthesis, through unknown molecular mechanisms by which it blocks synthesis [90]. This justifies our observation of a longer G1 phase and a short S phase in case of **R234** treated cells.

Gene expression profile analysis also revealed the increased levels of FOXO4, which negatively regulates the cell cycle, whereas low NRF2 increase chemo-sensitivity as well as stress-induced death susceptibility. **R234** also negatively regulates cell growth and differentiation via CREB, as indicated by low levels of CREBBP. **R234** effectively promotes cell apoptosis and cell cycle arrest via elevating p53 level, which is often downregulated in most cancers. The p53 gene exerts its effect via p21 by downregulating cell cycle proteins such as CCND, CCNE, CDK6 and E2F, as well as upregulating RBL2, HDAC as evident from our transcriptome analysis. Increase in p53 also affects other tumorigenic features such as promoting apoptosis via upregulation of pro-apoptotic genes like Noxa, Puma, Bim, FAS, BAX, PIDD and reducing proliferation and damage repair via downregulation of GADD45s, SESNs and BAX as supported by our results.

Further gene expression analysis also revealed the anti-cancer effects of **R234** via other pathways such as JAK-STAT pathway, as marked by downregulation of genes such as JAK1, STAT3, STAT1, GRB2, PIM1, CCND, also affecting the MAPK pathway and JNK pathway indicated by downregulation of significant genes such as JUN and FOS, decreasing angiogenesis and proliferation. In addition, the drug increase chemo-sensitivity by suppressing MITF, and affecting cytoskeletal proteins such as TUBB3, MCL1, ACTB and SPTAN1. Over all, inhibitory activity of PI3K/Akt/mTOR signaling pathway and cell cycle pathways were found and correlated with the cell death activation, which suggest that this class of compound might function by inhibiting multiple key proteins involved in the RTK signaling pathways. In addition, the top compound **R234 was identified to have** interactions with 11 amino acid residues of TrkA. The amino acid residues 313LEU and 314ARG formed hydrogen-bonding interactions with this compound. Compared all the tested compounds R234 had higher hydrogen

bonding interaction between the TrkA. Thus, newly synthesized compound R234 could be considered as promising RTK inhibitors for the development of potential anti-GBM drug.

Supplementary Materials

The following are available online, Figure S1… Table S1: Phenotypic characterization of cells from patient number 1, 2, 3 by immunofluorescence analysis.

Author Contributions

FZ and AG synthesized and characterized the compounds; AV and DK performed the *in vitro* experiments, and AM analyzed the RNA-seq data; FES supervised the gene expression and pathway analysis. MK and OY conceived and supervised the work, wrote and revised the manuscript. All authors approved the submitted version.

Funding

MK, AV and OYH acknowledge the Academy of Finland for the project grant support (decision no. 297200) and Tampere University of Technology for Instrumental facility grant support. The publication was prepared with the support of the "RUDN University Program 5-100".

Conflicts of Interest

The authors declare there are no conflict of interest.

REFERENCES:

[1] J. Chen, R.M. McKay, L.F. Parada, Malignant glioma: Lessons from genomics, mouse

models, and stem cells, Cell. (2012). doi:10.1016/j.cell.2012.03.009.

[2] C.W. Brennan, R.G.W. Verhaak, A. McKenna, B. Campos, H. Noushmehr, S.R. Salama, S. Zheng, D. Chakravarty, J.Z. Sanborn, S.H. Berman, R. Beroukhim, B. Bernard, C.J. Wu, G. Genovese, I. Shmulevich, J. Barnholtz-Sloan, L. Zou, R. Vegesna, S.A. Shukla, G. Ciriello, W.K. Yung, W. Zhang, C. Sougnez, T. Mikkelsen, K. Aldape, D.D. Bigner, E.G. Van Meir, M. Prados, A. Sloan, K.L. Black, J. Eschbacher, G. Finocchiaro, W. Friedman, D.W. Andrews, A. Guha, M. Iacocca, B.P. O'Neill, G. Foltz, J. Myers, D.J. Weisenberger, R. Penny, R. Kucherlapati, C.M. Perou, D.N. Hayes, R. Gibbs, M. Marra, G.B. Mills, E. Lander, P. Spellman, R. Wilson, C. Sander, J. Weinstein, M. Meyerson, S. Gabriel, P.W. Laird, D. Haussler, G. Getz, L. Chin, C. Benz, W. Barrett, Q. Ostrom, Y. Wolinsky, B. Bose, P.T. Boulos, M. Boulos, J. Brown, C. Czerinski, M. Eppley, T. Kempista, T. Kitko, Y. Koyfman, B. Rabeno, P. Rastogi, M. Sugarman, P. Swanson, K. Yalamanchii, I.P. Otey, Y.S. Liu, Y. Xiao, J.T. Auman, P.C. Chen, A. Hadjipanayis, E. Lee, S. Lee, P.J. Park, J. Seidman, L. Yang, S. Kalkanis, L.M. Poisson, A. Raghunathan, L. Scarpace, R. Bressler, A. Eakin, L. Iype, R.B. Kreisberg, K. Leinonen, S. Reynolds, H. Rovira, V. Thorsson, M.J. Annala, J. Paulauskis, E. Curley, M. Hatfield, D. Mallery, S. Morris, T. Shelton, C. Shelton, M. Sherman, P. Yena, L. Cuppini, F. DiMeco, M. Eoli, E. Maderna, B. Pollo, M. Saini, S. Balu, K.A. Hoadley, L. Li, C.R. Miller, Y. Shi, M.D. Topal, J. Wu, G. Dunn, C. Giannini, B.A. Aksoy, Y. Antipin, L. Borsu, E. Cerami, J. Gao, B. Gross, A. Jacobsen, M. Ladanyi, A. Lash, Y. Liang, B. Reva, N. Schultz, R. Shen, N.D. Socci, A. Viale, M.L. Ferguson, Q.R. Chen, J.A. Demchok, L.A.L. Dillon, K.R. Mills Shaw, M. Sheth, R. Tarnuzzer, Z. Wang, L. Yang, T. Davidsen, M.S. Guyer, B.A. Ozenberger, H.J. Sofia, J. Bergsten, J. Eckman, J. Harr, C. Smith, K. Tucker, C. Winemiller, L.A. Zach,

J.Y. Ljubimova, G. Eley, B. Ayala, M.A. Jensen, A. Kahn, T.D. Pihl, D.A. Pot, Y. Wan, N. Hansen, P. Hothi, B. Lin, N. Shah, J.G. Yoon, C. Lau, M. Berens, K. Ardlie, S.L. Carter, A.D. Cherniack, M. Noble, J. Cho, K. Cibulskis, D. DiCara, S. Frazer, S.B. Gabriel, N. Gehlenborg, J. Gentry, D. Heiman, J. Kim, R. Jing, E.S. Lander, M. Lawrence, P. Lin, W. Mallard, R.C. Onofrio, G. Saksena, S. Schumacher, P. Stojanov, B. Tabak, D. Voet, H. Zhang, N.N. Dees, L. Ding, L.L. Fulton, R.S. Fulton, K.L. Kanchi, E.R. Mardis, R.K. Wilson, S.B. Baylin, L. Harshyne, M.L. Cohen, K. Devine, A.E. Sloan, S.R. Van Den Berg, M.S. Berger, D. Carlin, B. Craft, K. Ellrott, M. Goldman, T. Goldstein, M. Grifford, S. Ma, S. Ng, J. Stuart, T. Swatloski, P. Waltman, J. Zhu, R. Foss, B. Frentzen, R. McTiernan, A. Yachnis, Y. Mao, R. Akbani, O. Bogler, G.N. Fuller, W. Liu, Y. Liu, Y. Lu, A. Protopopov, X. Ren, Y. Sun, W.K.A. Yung, J. Zhang, K. Chen, J.N. Weinstein, M.S. Bootwalla, P.H. Lai, T.J. Triche, D.J. Van Den Berg, D.H. Gutmann, N.L. Lehman, D. Brat, J.J. Olson, G.M. Mastrogianakis, N.S. Devi, Z. Zhang, E. Lipp, R. McLendon, The somatic genomic landscape of glioblastoma, Cell. 155 (2013). doi:10.1016/j.cell.2013.09.034.

[3] R. McLendon, A. Friedman, D. Bigner, E.G. Van Meir, D.J. Brat, G.M. Mastrogianakis, J.J. Olson, T. Mikkelsen, N. Lehman, K. Aldape, W.K.A. Yung, O. Bogler, J.N. Weinstein, S. VandenBerg, M. Berger, M. Prados, D. Muzny, M. Morgan, S. Scherer, A. Sabo, L. Nazareth, L. Lewis, O. Hall, Y. Zhu, Y. Ren, O. Alvi, J. Yao, A. Hawes, S. Jhangiani, G. Fowler, A. San Lucas, C. Kovar, A. Cree, H. Dinh, J. Santibanez, V. Joshi, M.L. Gonzalez-Garay, C.A. Miller, A. Milosavljevic, L. Donehower, D.A. Wheeler, R.A. Gibbs, K. Cibulskis, C. Sougnez, T. Fennell, S. Mahan, J. Wilkinson, L. Ziaugra, R. Onofrio, T. Bloom, R. Nicol, K. Ardlie, J. Baldwin, S. Gabriel, E.S. Lander, L. Ding, R.S.

Fulton, M.D. McLellan, J. Wallis, D.E. Larson, X. Shi, R. Abbott, L. Fulton, K. Chen, D.C. Koboldt, M.C. Wendl, R. Meyer, Y. Tang, L. Lin, J.R. Osborne, B.H. Dunford-Shore, T.L. Miner, K. Delehaunty, C. Markovic, G. Swift, W. Courtney, C. Pohl, S. Abbott, A. Hawkins, S. Leong, C. Haipek, H. Schmidt, M. Wiechert, T. Vickery, S. Scott, D.J. Dooling, A. Chinwalla, G.M. Weinstock, E.R. Mardis, R.K. Wilson, G. Getz, W. Winckler, R.G.W. Verhaak, M.S. Lawrence, M. O'Kelly, J. Robinson, G. Alexe, R. Beroukhim, S. Carter, D. Chiang, J. Gould, S. Gupta, J. Korn, C. Mermel, J. Mesirov, S. Monti, H. Nguyen, M. Parkin, M. Reich, N. Stransky, B.A. Weir, L. Garraway, T. Golub, M. Meyerson, L. Chin, A. Protopopov, J. Zhang, I. Perna, S. Aronson, N. Sathiamoorthy, G. Ren, J. Yao, W.R. Wiedemeyer, H. Kim, W.K. Sek, Y. Xiao, I.S. Kohane, J. Seidman, P.J. Park, R. Kucherlapati, P.W. Laird, L. Cope, J.G. Herman, D.J. Weisenberger, F. Pan, D. Van Den Berg, L. Van Neste, M.Y. Joo, K.E. Schuebel, S.B. Baylin, D.M. Absher, J.Z. Li, A. Southwick, S. Brady, A. Aggarwal, T. Chung, G. Sherlock, J.D. Brooks, R.M. Myers, P.T. Spellman, E. Purdom, L.R. Jakkula, A. V. Lapuk, H. Marr, S. Dorton, G.C. Yoon, J. Han, A. Ray, V. Wang, S. Durinck, M. Robinson, N.J. Wang, K. Vranizan, V. Peng, E. Van Name, G. V. Fontenay, J. Ngai, J.G. Conboy, B. Parvin, H.S. Feiler, T.P. Speed, J.W. Gray, C. Brennan, N.D. Socci, A. Olshen, B.S. Taylor, A. Lash, N. Schultz, B. Reva, Y. Antipin, A. Stukalov, B. Gross, E. Cerami, Q.W. Wei, L.X. Qin, V.E. Seshan, L. Villafania, M. Cavatore, L. Borsu, A. Viale, W. Gerald, C. Sander, M. Ladanyi, C.M. Perou, D.N. Hayes, M.D. Topal, K.A. Hoadley, Y. Qi, S. Balu, Y. Shi, J. Wu, R. Penny, M. Bittner, T. Shelton, E. Lenkiewicz, S. Morris, D. Beasley, S. Sanders, A. Kahn, R. Sfeir, J. Chen, D. Nassau, L. Feng, E. Hickey, A. Barker, D.S. Gerhard, J. Vockley, C. Compton, J. Vaught, P. Fielding, M.L. Ferguson, C. Schaefer, J. Zhang, S. Madhavan,

K.H. Buetow, F. Collins, P. Good, M. Guyer, B. Ozenberger, J. Peterson, E. Thomson, Comprehensive genomic characterization defines human glioblastoma genes and core pathways, Nature. (2008). doi:10.1038/nature07385.

[4] P. Blume-Jensen, T. Hunter, Oncogenic kinase signalling, Nature. (2001). doi:10.1038/35077225.

[5] N.J. Szerlip, A. Pedraza, D. Chakravarty, M. Azim, J. McGuire, Y. Fang, T. Ozawa, E.C. Holland, J.T. Huse, S. Jhanwar, M.A. Leversha, T. Mikkelsen, C.W. Brennan, Intratumoral heterogeneity of receptor tyrosine kinases EGFR and PDGFRA amplification in glioblastoma defines subpopulations with distinct growth factor response, Proc. Natl. Acad. Sci. (2012). doi:10.1073/pnas.1114033109.

[6] J.M. Stommel, A.C. Kimmelman, H. Ying, R. Nabioullin, A.H. Ponugoti, R. Wiedemeyer, A.H. Stegh, J.E. Bradner, K.L. Ligon, C. Brennan, L. Chin, R. a DePinho, Coactivation of receptor tyrosine kinases affects the response of tumor cells to targeted therapies., Science. (2007). doi:10.1126/science.1142946.

[7] T. Regad, Targeting RTK signaling pathways in cancer, Cancers (Basel). (2015). doi:10.3390/cancers7030860.

[8] S. Lawn, N. Krishna, A. Pisklakova, X. Qu, D.A. Fenstermacher, M. Fournier, F.D. Vrionis, N. Tran, J.A. Chan, R.S. Kenchappa, P.A. Forsyth, Neurotrophin Signaling via TrkB and TrkC Receptors Promotes the Growth of Brain Tumor-initiating Cells, J. Biol. Chem. (2015). doi:10.1074/jbc.M114.599373.

[9] S. Wadhwa, T.C. Nag, A. Jindal, R. Kushwaha, A.K. Mahapatra, C. Sarkar, Expression of the neurotrophin receptors Trk A and Trk B in adult human astrocytoma and glioblastoma,

J. Biosci. (2003). doi:10.1007/BF02706217.

[10] M. Bassili, E. Birman, N.F. Schor, H.U. Saragovi, Differential roles of Trk and p75 neurotrophin receptors in tumorigenesis and chemoresistance ex vivo and in vivo, Cancer Chemother. Pharmacol. (2010). doi:10.1007/s00280-009-1110-x.

[11] D.E. Bredesen, S. Rabizadeh, p75(NTR) and apoptosis: Trk-dependent and Trk-independent effects, Trends Neurosci. (1997). doi:10.1016/S0166-2236(96)01049-1.

[12] M. Barbacid, The Trk family of neurotrophin receptors, J. Neurobiol. (1994). doi:10.1002/neu.480251107.

[13] Y. Wang, C. Hagel, W. Hamel, S. Müller, L. Kluwe, M. Westphal, Trk A, B, and C are commonly expressed in human astrocytes and astrocytic gliomas but not by human oligodendrocytes and oligodendroglioma, Acta Neuropathol. (1998). doi:10.1007/s004010050906.

[14] A.M. Lange, H.W. Lo, Inhibiting TRK proteins in clinical cancer therapy, Cancers (Basel). (2018). doi:10.3390/cancers10040105.

[15] J. Meldolesi, Neurotrophin Trk Receptors: New Targets for Cancer Therapy., Rev. Physiol. Biochem. Pharmacol. (2017). doi:10.1007/112_2017_6.

[16] J.J. Gentry, P. Casaccia-Bonnefil, B.D. Carter, Nerve growth factor activation of nuclear factor ??B through its p75 receptor is an anti-apoptotic signal in RN22 schwannoma cells, J. Biol. Chem. (2000). doi:10.1074/jbc.275.11.7558.

[17] A. Chittka, J.C. Arevalo, M. Rodriguez-Guzman, P. Pérez, M. V. Chao, M. Sendtner, The p75NTR-interacting protein SC1 inhibits cell cycle progression by transcriptional

repression of cyclin E, J. Cell Biol. (2004). doi:10.1083/jcb.200301106.

[18] A. Nykjaer, R. Lee, K.K. Teng, P. Jansen, P. Madsen, M.S. Nielsen, C. Jacobsen, M. Kliemannel, E. Schwarz, T.E. Willnow, B.L. Hempstead, C.M. Petersen, Sortilin is essential for proNGF-induced neuronal cell death, Nature. (2004). doi:10.1038/nature02319.

[19] S. Rabizadeh, S. Rabizadeh, X. Ye, J.J.L. Wang, D.E. Bredesen, Neurotrophin dependence mediated by p75(NTR): Contrast between rescue by BDNF and NGF, Cell Death Differ. (1999). doi:10.1038/sj.cdd.4400614.

[20] L. Notterpek, Neurotrophins in myelination: A new role for a puzzling receptor, Trends Neurosci. (2003). doi:10.1016/S0166-2236(03)00099-7.

[21] B.D. Carter, C. Kaltschmidt, B. Kaltschmidt, N. Offenhauser, R. Bohm-Matthaei, P.A. Baeuerle, Y.A. Barde, Selective activation of NF-kappa B by nerve growth factor through the neurotrophin receptor p75, Science (80-.). (1996). doi:10.1126/science.272.5261.542.

[22] X. Zhou, Q. Hao, P. Liao, S. Luo, M. Zhang, G. Hu, H. Liu, Y. Zhang, B. Cao, M. Baddoo, E.K. Flemington, S.X. Zeng, H. Lu, Nerve growth factor receptor negates the tumor suppressor p53 as a feedback regulator, Elife. (2016). doi:10.7554/eLife.15099.

[23] S. Verbeke, E. Tomellini, F. Dhamani, S. Meignan, E. Adriaenssens, L.B. Xuefen, Extracellular cleavage of the p75 neurotrophin receptor is implicated in its pro-survival effect in breast cancer cells, FEBS Lett. (2013). doi:10.1016/j.febslet.2013.06.039.

[24] I. Charalampopoulos, A. Vicario, I. Pediaditakis, A. Gravanis, A. Simi, C.F. Ibáñez, Genetic Dissection of Neurotrophin Signaling through the p75 Neurotrophin Receptor,

Cell Rep. (2012). doi:10.1016/j.celrep.2012.11.009.

[25] Y. Hayakawa, K. Sakitani, M. Konishi, S. Asfaha, R. Niikura, H. Tomita, B.W. Renz, Y. Tailor, M. Macchini, M. Middelhoff, Z. Jiang, T. Tanaka, Z.A. Dubeykovskaya, W. Kim, X. Chen, A.M. Urbanska, K. Nagar, C.B. Westphalen, M. Quante, C.S. Lin, M.D. Gershon, A. Hara, C.M. Zhao, D. Chen, D.L. Worthley, K. Koike, T.C. Wang, Nerve Growth Factor Promotes Gastric Tumorigenesis through Aberrant Cholinergic Signaling, Cancer Cell. (2017). doi:10.1016/j.ccell.2016.11.005.

[26] C. Festuccia, P. Muzi, G.L. Gravina, D. Millimaggi, S. Speca, V. Dolo, E. Ricevuto, C. Vicentini, M. Bologna, Tyrosine kinase inhibitor CEP-701 blocks the NTRK1/NGF receptor and limits the invasive capability of prostate cancer cells in vitro, Int. J. Oncol. (2007).

[27] S. Yust-Katz, D. Liu, Y. Yuan, V. Liu, S. Kang, M. Groves, V. Puduvalli, V. Levin, C. Conrad, H. Colman, S. Hsu, W.K.A. Yung, M.R. Gilbert, Phase 1/1b study of lonafarnib and temozolomide in patients with recurrent or temozolomide refractory glioblastoma, Cancer. (2013). doi:10.1002/cncr.28031.

[28] E. Carra, F. Barbieri, D. Marubbi, A. Pattarozzi, R.E. Favoni, T. Florio, A. Daga, Sorafenib selectively depletes human glioblastoma tumor-initiating cells from primary cultures, Cell Cycle. (2013). doi:10.4161/cc.23372.

[29] T.N. Kreisl, L. Kim, K. Moore, P. Duic, C. Royce, I. Stroud, N. Garren, M. Mackey, J.A. Butman, K. Camphausen, J. Park, P.S. Albert, H.A. Fine, Phase II trial of single-agent bevacizumab followed by bevacizumab plus irinotecan at tumor progression in recurrent glioblastoma, J. Clin. Oncol. (2009). doi:10.1200/JCO.2008.16.3055.

[30] N. Butowski, S.M. Chang, K.R. Lamborn, M.Y. Polley, R. Pieper, J.F. Costello, S. Vandenberg, R. Parvataneni, A. Nicole, P.K. Sneed, J. Clarke, E. Hsieh, B.M. Costa, R.M. Reis, M. Hristova-Kazmierski, S.J. Nicol, D.E. Thornton, M.D. Prados, Phase II and pharmacogenomics study of enzastaurin plus temozolomide during and following radiation therapy in patients with newly diagnosed glioblastoma multiforme and gliosarcoma, Neuro. Oncol. (2011). doi:10.1093/neuonc/nor130.

[31] D.A. Reardon, B. Neyns, M. Weller, J.C. Tonn, L.B. Nabors, R. Stupp, Cilengitide: An RGD pentapeptide αvβ3 and αvβ5 integrin inhibitor in development for glioblastoma and other malignancies, Futur. Oncol. (2011). doi:10.2217/fon.11.8.

[32] B. Jutten, L. Dubois, Y. Li, H. Aerts, B.G. Wouters, P. Lambin, J. Theys, G. Lammering, Binding of cetuximab to the EGFRvIII deletion mutant and its biological consequences in malignant glioma cells, Radiother. Oncol. (2009). doi:10.1016/j.radonc.2009.06.021.

[33] J. Mendelsohn, J. Baselga, Epidermal Growth Factor Receptor Targeting in Cancer, Semin. Oncol. (2006). doi:10.1053/j.seminoncol.2006.04.003.

[34] E. Arwert, S. Hingtgen, J.L. Figueiredo, H. Bergquist, U. Mahmood, R. Weissleder, K. Shah, Visualizing the dynamics of EGFR activity and antiglioma therapies in vivo, Cancer Res. (2007). doi:10.1158/0008-5472.CAN-07-0077.

[35] S.A. Greenall, J.F. Donoghue, M. Van Sinderen, V. Dubljevic, S. Budiman, M. Devlin, I. Street, T.E. Adams, T.G. Johns, EGFRvIII-mediated transactivation of receptor tyrosine kinases in glioma: Mechanism and therapeutic implications, Oncogene. (2015). doi:10.1038/onc.2014.448.

[36] E. Ranza, G. Mazzini, A. Facoetti, R. Nano, In-vitro effects of the tyrosine kinase

inhibitor imatinib on glioblastoma cell proliferation, J. Neurooncol. (2010). doi:10.1007/s11060-009-9975-4.

[37] J. Drukala, K. Urbanska, A. Wilk, M. Grabacka, E. Wybieralska, L. Del Valle, Z. Madeja, K. Reiss, ROS accumulation and IGF-IR inhibition contribute to fenofibrate/PPARα -mediated inhibition of Glioma cell motility in vitro, Mol. Cancer. (2010). doi:10.1186/1476-4598-9-159.

[38] E. Carrasco-García, M. Saceda, I. Martínez-Lacaci, Role of Receptor Tyrosine Kinases and Their Ligands in Glioblastoma, Cells. (2014). doi:10.3390/cells3020199.

[39] D.R. Premkumar, E.P. Jane, I.F. Pollack, Co-administration of NVP-AEW541 and dasatinib induces mitochondrial- mediated apoptosis through Bax activation in malignant human glioma cell lines, Int. J. Oncol. (2010). doi:10.3892/ijo-00000712.

[40] A. Chakravarti, J.S. Loeffler, N.J. Dyson, Insulin-like growth factor receptor I mediates resistance to anti-epidermal growth factor receptor therapy in primary human glioblastoma cells through continued activation of phosphoinositide 3-kinase signaling, Cancer Res. (2002).

[41] S.K. Sridhar, S.N. Pandeya, J.P. Stables, A. Ramesh, Anticonvulsant activity of hydrazones, Schiff and Mannich bases of isatin derivatives, Eur. J. Pharm. Sci. 16 (2002) 129–132. doi:10.1016/S0928-0987(02)00077-5.

[42] R. Sinha, U.V.S. Sara, R.L. Khosa, J. Stables, J. Jain, Nicotinic acid hydrazones: A novel anticonvulsant pharmacophore, in: Med. Chem. Res., 2011: pp. 1499–1504. doi:10.1007/s00044-010-9396-0.

[43] S. Rollas, Ş.G. Küçükgüzel, Biological activities of hydrazone derivatives, Molecules. 12 (2007) 1910–1939. doi:10.3390/12081910.

[44] S.N. Pandeya, H. Manjula, P.N. Singh, Antidepressant activity of some phenylaceticacid hydrazones and 2-chlorophenyl semicarbazones [4], Indian J. Physiol. Pharmacol. 44 (2000) 509–510.

[45] S. Neha, R. Ritu, K. Manju, K. Birendra, A review on biological activities of hydrazone derivatives, Int. J. Pharm. Clin. Res. 8 (2016) 162–166.

[46] C.L. S, Analgesic and anti-inflammatory potential of hydrazones, J. Chem. Pharm. Res. 6 (2014) 916–934. http://www.jocpr.com/articles/analgesic-and-antiinflammatory-potential-of-hydrazones.pdf.

[47] N.A. Hamdy, H.A. Abdel-Aziz, G.M. Kamel, I.M.I. Fakhr, Convenient synthesis, anti-inflammatory, analgesic and ulcerogenic activites of some new bis-hydrazones and pyrazole derivatives, Acta Pol. Pharm. - Drug Res. 70 (2013) 469–480.

[48] A. Kajal, S. Bala, N. Sharma, S. Kamboj, V. Saini, Therapeutic Potential of Hydrazones as Anti-Inflammatory Agents, Int. J. Med. Chem. 2014 (2014) 1–11. doi:10.1155/2014/761030.

[49] C.M. Moldovan, O. Oniga, A. Pârvu, B. Tiperciuc, P. Verite, A. Pîrnău, O. Crişan, M. Bojiţă, R. Pop, Synthesis and anti-inflammatory evaluation of some new acyl-hydrazones bearing 2-aryl-thiazole, Eur. J. Med. Chem. 46 (2011) 526–534. doi:10.1016/j.ejmech.2010.11.032.

[50] F.R. Pavan, P.I. d. S. Maia, S.R.A. Leite, V.M. Deflon, A.A. Batista, D.N. Sato, S.G.

Franzblau, C.Q.F. Leite, Thiosemicarbazones, semicarbazones, dithiocarbazates and hydrazide/hydrazones: Anti - Mycobacterium tuberculosis activity and cytotoxicity, Eur. J. Med. Chem. 45 (2010) 1898–1905. doi:10.1016/j.ejmech.2010.01.028.

[51] M.T. Cocco, C. Congiu, V. Lilliu, V. Onnis, Synthesis and in vitro antitumoral activity of new hydrazinopyrimidine-5-carbonitrile derivatives, Bioorg. Med. Chem. 14 (2006) 366–372. doi:10.1016/j.bmc.2005.08.012.

[52] M.S. Alam, D.U. Lee, Synthesis, biological evaluation, drug-likeness, and in silico screening of novel benzylidene-hydrazone analogues as small molecule anticancer agents, Arch. Pharm. Res. 39 (2016) 191–201. doi:10.1007/s12272-015-0699-z.

[53] R. Nitsch, I. Bechmann, R.A. Deisz, D. Haas, T.N. Lehmann, U. Wendling, F. Zipp, Human brain-cell death induced by tumour-necrosis-factor-related apoptosis-inducing ligand (TRAIL), Lancet. (2000). doi:10.1016/S0140-6736(00)02659-3.

[54] A.P. Demchenko, Beyond annexin V: Fluorescence response of cellular membranes to apoptosis, Cytotechnology. (2013). doi:10.1007/s10616-012-9481-y.

[55] G. Zhang, V. Gurtu, S.R. Kain, G. Yan, Early detection of apoptosis using a fluorescent conjugate of annexin V, Biotechniques. (1997). doi:10.2144/97233pf01.

[56] R. Hingorani, J. Deng, J. Elia, C. McIntyre, D. Mittar, Detection of Apoptosis Using the BD Annexin V FITC Assay on the BD FACSVerse^{TM} System, BD Biosci. (2011).

[57] A.K. Hagan, T. Zuchner, Lanthanide-based time-resolved luminescence immunoassays, Anal. Bioanal. Chem. (2011). doi:10.1007/s00216-011-5047-7.

[58] S. Palanivel, A. Zhurina, P. Doan, J.G. Chandraseelan, V.K.M. Khandelwal, F.I. Zubkov,

K.T. Mahmudov, A.J.L. Pombeiro, O. Yli-Harja, M. Kandhavelu, In vitro characterization of arylhydrazones of active methylene derivatives., Saudi Pharm. J. SPJ Off. Publ. Saudi Pharm. Soc. 26 (2018) 430–436. doi:10.1016/j.jsps.2017.12.018.

[59] G. Xu, M.C. Abad, P.J. Connolly, M.P. Neeper, G.T. Struble, B.A. Springer, S.L. Emanuel, N. Pandey, R.H. Gruninger, M. Adams, S. Moreno-Mazza, A.R. Fuentes-Pesquera, S.A. Middleton, 4-Amino-6-arylamino-pyrimidine-5-carbaldehyde hydrazones as potent ErbB-2/EGFR dual kinase inhibitors, Bioorganic Med. Chem. Lett. (2008). doi:10.1016/j.bmcl.2008.07.020.

[60] S.M. Abou-Seri, Synthesis and biological evaluation of novel 2,4′-bis substituted diphenylamines as anticancer agents and potential epidermal growth factor receptor tyrosine kinase inhibitors, Eur. J. Med. Chem. (2010). doi:10.1016/j.ejmech.2010.05.072.

[61] K.T. Mahmudov, M.N. Kopylovich, A. Sabbatini, M.G.B. Drew, L.M.D.R.S. Martins, C. Pettinari, A.J.L. Pombeiro, Cooperative metal-ligand assisted E/Z isomerization and cyano activation at CuIIand CoIIcomplexes of arylhydrazones of active methylene nitriles, Inorg. Chem. (2014). doi:10.1021/ic501704g.

[62] K.T. Mahmudov, M.F.C.G. Da Silva, M. Sutradhar, M.N. Kopylovich, F.E. Huseynov, N.T. Shamilov, A.A. Voronina, T.M. Buslaeva, A.J.L. Pombeiro, Lanthanide derivatives comprising arylhydrazones of β-diketones: Cooperative E/Z isomerization and catalytic activity in nitroaldol reaction, Dalt. Trans. (2015). doi:10.1039/c4dt03788j.

[63] K.T. Mahmudov, A.M. Maharramov, R.A. Aliyeva, I.A. Aliyev, R.K. Askerov, R. Batmaz, M.N. Kopylovich, A.J.L. Pombeiro, 3-(para-Substituted phenylhydrazo)pentane-2,4-diones: Physicochemical and solvatochromic properties, J. Photochem. Photobiol. A

Chem. (2011). doi:10.1016/j.jphotochem.2011.02.006.

[64] K.T. Mahmudov, A.M. Maharramov, R.A. Aliyeva, I.A. Aliyev, M.N. Kopylovich, A.J.L. Pombeiro, Ion pairs of 5,5-dimethyl-2-(2-hydroxy-3,5-disulfophenylhydrazo)cyclohexane-1,3-dione with cationic surface-active substances as analytical reagent for determination of copper(II), Anal. Lett. (2010). doi:10.1080/00032711003763665.

[65] M.N. Kopylovich, K.T. Mahmudov, A. Mizar, A.J.L. Pombeiro, Hydrogen bond assisted activation of a dinitrile towards nucleophilic attack, Chem. Commun. (2011). doi:10.1039/c1cc11696g.

[66] C.A. Montoya, C.F. Gómez, A.B. Paninho, A.V.M. Nunes, K.T. Mahmudov, V. Najdanovic-Visak, L.M.D.R.S. Martins, M.F.C. Guedes Da Silva, A.J.L. Pombeiro, M. Nunes Da Ponte, Cyclic carbonate synthesis from CO2and epoxides using zinc(II) complexes of arylhydrazones of β-diketones, J. Catal. (2016). doi:10.1016/j.jcat.2015.12.027.

[67] A. Karmakar, A. Paul, K.T. Mahmudov, M.F.C. Guedes Da Silva, A.J.L. Pombeiro, PH dependent synthesis of Zn(ii) and Cd(ii) coordination polymers with dicarboxyl-functionalized arylhydrazone of barbituric acid: Photoluminescence properties and catalysts for Knoevenagel condensation, New J. Chem. (2016). doi:10.1039/c5nj02411k.

[68] M.N. Kopylovich, A.C.C. Nunes, K.T. Mahmudov, M. Haukka, T.C.O. Mac Leod, L.M.D.R.S. Martins, M.L. Kuznetsov, A.J.L. Pombeiro, Complexes of copper(II) with 3-(ortho-substituted phenylhydrazo)pentane-2,4-diones: syntheses, properties and catalytic activity for cyclohexane oxidation., Dalton Trans. (2011). doi:10.1039/c0dt01527j.

[69] W. Kuznik, M.N. Kopylovich, G.I. Amanullayeva, A.J.L. Pombeiro, A.H. Reshak, K.T. Mahmudov, I. V. Kityk, Role of tautomerism and solvatochromism in UV-VIS spectra of arylhydrazones of β-diketones, J. Mol. Liq. (2012). doi:10.1016/j.molliq.2012.03.023.

[70] K.T. Mahmudov, M.F.C. Guedes Da Silva, M. Glucini, M. Renzi, K.C.P. Gabriel, M.N. Kopylovich, M. Sutradhar, F. Marchetti, C. Pettinari, S. Zamponi, A.J.L. Pombeiro, Water-soluble heterometallic copper(II)-sodium complex comprising arylhydrazone of barbituric acid as a ligand, Inorg. Chem. Commun. (2012). doi:10.1016/j.inoche.2012.06.008.

[71] K.T. Mahmudov, R.A. Rahimov, M.B. Babanly, P.Q. Hasanov, F.G. Pashaev, A.G. Gasanov, M.N. Kopylovich, A.J.L. Pombeiro, Tautomery and acid-base properties of some azoderivatives of benzoylacetone, J. Mol. Liq. (2011). doi:10.1016/j.molliq.2011.06.005.

[72] K.T. Mahmudov, M.N. Kopylovich, K. V. Luzyanin, A. Mizar, M.F.C. Guedes Da Silva, V. André, A.J.L. Pombeiro, Structural and thermal properties of three cyano-substituted azoderivatives of β-diketones, J. Mol. Struct. (2011). doi:10.1016/j.molstruc.2011.02.045.

[73] M.N. Kopylovich, K.T. Mahmudov, M.F.C. Guedes Da Silva, L.M.D.R.S. Martins, M.L. Kuznetsov, T.F.S. Silva, J.J.R. Fraústo Da Silva, A.J.L. Pombeiro, Trends in properties of para-substituted 3-(phenylhydrazo)pentane-2,4- diones, J. Phys. Org. Chem. (2011). doi:10.1002/poc.1824.

[74] K.T. Mahmudov, M.N. Kopylovich, M.F.C. Guedes Da Silva, G.S. Mahmudova, M. Sutradhar, A.J.L. Pombeiro, Copper(II) and cobalt(II,III) complexes of a new carboxylic-functionalized arylhydrazone of 5,5-dimethylcyclohexane-1, 3-dione, Polyhedron. (2013).

doi:10.1016/j.poly.2013.05.027.

[75] W.L. Jorgensen, D.S. Maxwell, J. Tirado-Rives, Development and testing of the OPLS all-atom force field on conformational energetics and properties of organic liquids, J. Am. Chem. Soc. (1996). doi:10.1021/ja9621760.

[76] a G. Robertson, M.J. Banfield, S.J. Allen, J. a Dando, G.G. Mason, S.J. Tyler, G.S. Bennett, S.D. Brain, a R. Clarke, R.L. Naylor, G.K. Wilcock, R.L. Brady, D. Dawbarn, Identification and structure of the nerve growth factor binding site on TrkA., Biochem. Biophys. Res. Commun. (2001). doi:10.1006/bbrc.2001.4462.

[77] J. Moungjaroen, U. Nimmannit, P.S. Callery, L. Wang, N. Azad, V. Lipipun, P. Chanvorachote, Y. Rojanasakul, Reactive oxygen species mediate caspase activation and apoptosis induced by lipoic acid in human lung epithelial cancer cells through Bcl-2 down-regulation., J. Pharmacol. Exp. Ther. 319 (2006) 1062–1069. doi:10.1124/jpet.106.110965.glutathione.

[78] M. Redza-Dutordoir, D.A. Averill-Bates, Activation of apoptosis signalling pathways by reactive oxygen species, Biochim. Biophys. Acta - Mol. Cell Res. (2016). doi:10.1016/j.bbamcr.2016.09.012.

[79] K. Izeradjene, L. Douglas, D.M. Tillman, A.B. Delaney, J.A. Houghton, Reactive oxygen species regulate caspase activation in tumor necrosis factor-related apoptosis-inducing ligand-resistant human colon carcinoma cell lines, Cancer Res. 65 (2005) 7436–7445. doi:10.1158/0008-5472.CAN-04-2628.

[80] D.R. Ciocca, S.K. Calderwood, Heat shock proteins in cancer: Diagnostic, prognostic, predictive, and treatment implications, Cell Stress Chaperones. (2005). doi:10.1379/CSC-

99r.1.

[81] A. Sami, M. Karsy, Targeting the PI3K/AKT/mTOR signaling pathway in glioblastoma: Novel therapeutic agents and advances in understanding, Tumor Biol. (2013). doi:10.1007/s13277-013-0800-5.

[82] Z. Duzgun, Z. Eroglu, C. Biray Avci, Role of mTOR in glioblastoma, Gene. (2016). doi:10.1016/j.gene.2015.08.060.

[83] X. Li, C. Wu, N. Chen, H. Gu, A. Yen, L. Cao, E. Wang, L. Wang, PI3K/Akt/mTOR signaling pathway and targeted therapy for glioblastoma, Oncotarget. (2016). doi:10.18632/oncotarget.7961.

[84] M. Alam, G. Verma, M. Shaquiquzzaman, A. Marella, M. Akhtar, M. Ali, A review exploring biological activities of hydrazones, J. Pharm. Bioallied Sci. 6 (2014) 69. doi:10.4103/0975-7406.129170.

[85] M. Singh, N. Raghav, Biological activities of hydrazones: A review, Int. J. Pharm. Pharm. Sci. 3 (2011) 26–32. doi:10.1186/1752-153X-5-2; Rollas, S., Kiiciikguzel, S.G., Biological Activities of Hydrazone Derivatives (2007) Molecules, 12, pp. 1910-1939; Yadav, J., Pandeya, S.N., Nath, G., Singh, S.P., Synthesis and antibacterial evaluation of some hydrazones of flavanoid derivatives (2010) J Chem Pharm Res, 2 (4), pp. 558-563; Khan, S.U., Mullick, P., Pandit, S., Kaushik, D., Synthesis of hydrazones derivatives of Quinoxaline-prospective antimicrobial and anti-inflammatory agents (2009) Acta Polonica Pharmac.

[86] M.C. Mandewale, U.C. Patil, S. V. Shedge, U.R. Dappadwad, R.S. Yamgar, A review on quinoline hydrazone derivatives as a new class of potent antitubercular and anticancer

agents, Beni-Suef Univ. J. Basic Appl. Sci. (2017). doi:10.1016/j.bjbas.2017.07.005.

[87] H.S. Naveen Kumar, T. Parumasivam, F. Jumaat, P. Ibrahim, M.Z. Asmawi, A. Sadikun, Synthesis and evaluation of isonicotinoyl hydrazone derivatives as antimycobacterial and anticancer agents, Med. Chem. Res. 23 (2014) 269–279. doi:10.1007/s00044-013-0632-2.

[88] R.M. Mohareb, D.H. Fleita, O.K. Sakka, Novel synthesis of hydrazide-hydrazone derivatives and their utilization in the synthesis of coumarin, pyridine, thiazole and thiophene derivatives with antitumor activity, Molecules. (2011). doi:10.3390/molecules16010016.

[89] N. Dyson, The regulation of E2F by pRB-family proteins, Genes Dev. (1998). doi:10.1101/gad.12.15.2245.

[90] D. Avni, H. Yang, F. Martelli, F. Hofmann, W.M. ElShamy, S. Ganesan, R. Scully, D.M. Livingston, Active localization of the retinoblastoma protein in chromatin and its response to S phase DNA damage, Mol. Cell. (2003). doi:10.1016/S1097-2765(03)00355-1.

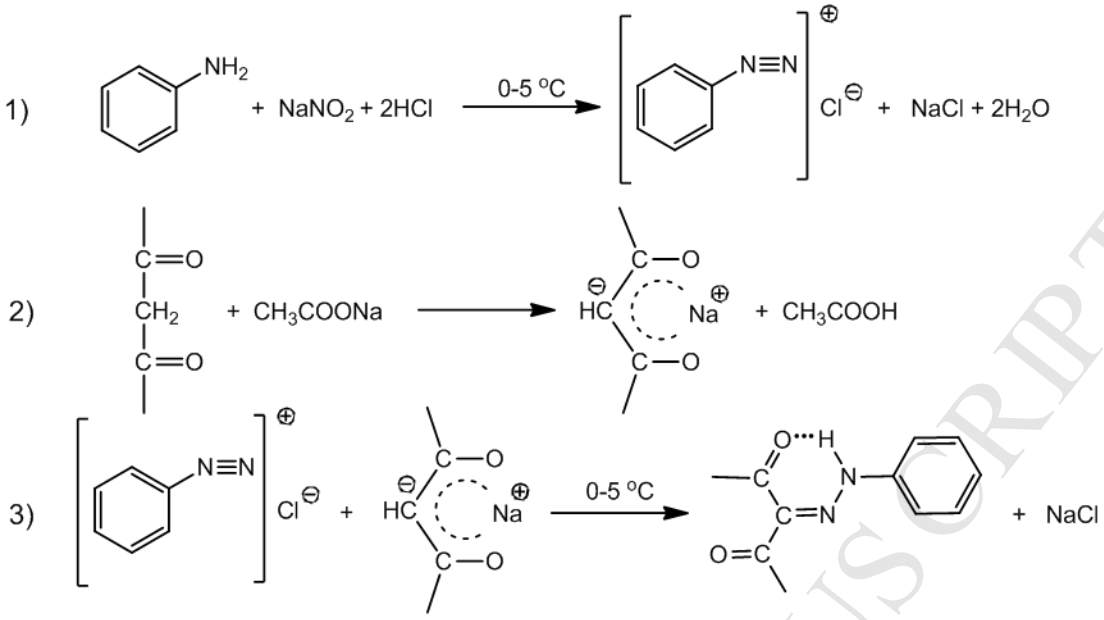

Highlights

- 2-(2-(2,4-dioxopentan-3-ylidene)hydrazineyl)benzonitrile, R234, effectively reduced GBM cells viability and proliferation at micro molar level.
- In U87 cells, R234 induced oxidative effects whereas LN229 cells annulled oxidative stress.
- R234 was found to exert its apoptotic effects independent of caspase3/7 activity, in GBM cell lines.
- R234 inhibits NGFR-mediated negative regulation of p53 signaling pathway
- R234 inhibits PI3K/Akt/mTOR signaling pathways of GBM cells